ENGINEERING REPORT

THE SPATIAL DISTRIBUTION PATTERNS OF SNOW WATER EQUIVALENT DATA FOR THE ACCUMULATION PHASE ACROSS THE SOUTHERN ROCKY MOUNTAINS

Submitted by

Isaac J. Y. Schrock

Department of Civil Engineering

In partial fulfillment of the requirements

For the Degree of Master of Science

Colorado State University

Fort Collins, Colorado

Fall 2020

Master's Committee:

Advisor: Neil Grigg

Steven R. Fassnacht (Technical Advisor)
Sybil Sharvelle (Committee Member)

ABSTRACT
The spatial characteristics and patterns of snow accumulation and ablation are used to estimate runoff volume, and timing of snowpack in mountainous regions across the western United States. This paper focuses on quantifying and characterizing the snow accumulation phase to investigate the spatio-temporal snow water equivalent (SWE) distribution in the Southern Rocky Mountains (SRM). Average daily SWE data were obtained from 90 Natural Resources Conservation Service (NRCS) Snow Telemetry (SNOTEL) data stations from southern Wyoming to northern New Mexico for the snow years between from 1982 to 2015. The stations range in elevation between 2268 and 3536 meters, and they were aggregated into seven sub-sets, based on elevation (high-low), latitude (north-south) and annual maximum SWE (above average, average, below average snow years).

For the entire dataset and the seven data sub-sets, the standard deviation versus mean trajectories were developed. Each trajectory was comprised of average daily data points across the snow year, and each data point represented the standard deviation and mean SWE values from a sub-set of the SNOTEL stations. The trajectory can be used to describe and represent the change in the snowpack over the water year. Within each trajectory, the accumulation (increasing snowpack), hysteretic (increasing and decreasing snowpack) and ablation (decreasing snowpack) phases can be observed, characterized and modeled. For this paper, regression techniques were applied to the accumulation phase only. The regression form, average slope, maximum slope, minimum slope, and coefficient of determination values were extracted. These data were aggregated across elevation, latitude and snow year sub-sets, and spatial patterns were evaluated.

Although the prior study (Egli and Jonas, 2009) used snow depth data, SWE data were the focus for this study. SWE data were available for a longer period of record than snow depth data in the SRM, and since SWE measures the mass of water rather the than depth snow, the physical effects of snow settling were eliminated from the analysis. The snow settling signature appeared in the data as noise in the standard deviation versus mean depth trajectory plots, compared to SWE trajectory plots. The removal of this noise, i.e., use of SWE trajectory plots, yielded stronger correlations than were produced using snow depth data.

The accumulation phase data most closely fit a truncated linear regression model, with the average slopes ranging between 0.36 to 0.40 (seven sub-sets), and the average standard deviation values ranging between 0.042 to 0.097. While the average accumulation slopes were fairly similar across all seven sub-sets, latitude impacted snowpack variability more significantly than did elevation. Within individual years, the accumulation snowpack in the south region was frequently more homogenous than the north region, but when aggregated across the 34-year study, the accumulation snowpack in the south region was less consistent on an inter-annual basis. In contrast to original hypotheses, when SWE were discretized by both elevation and latitude, the standard deviation of the accumulation slopes increased, rather than decreased. Snow year (above average, average, below average) was found to have a negligible impact on spatial homogeneity of the accumulation snowpack, except within the south-high sub-set, where range in average accumulation slope was 0.10. Generally, the snowpack was found to be more homogenous for below average snow years

compared to average or above average snow years, because below average snow years exhibited the lowest average accumulation slopes of the three categories.

TABLE OF CONTENTS

1.0 INTRODUCTION

Across the western United States, human existence and economic activity are defined by and centered on the availability or scarcity of water (Kearney et al., 2014). In the Southern Rocky Mountains (Colorado, Southern Wyoming and Northern New Mexico), the snowpack is the dominant contributor to surface water flows, and in Colorado surface water was estimated to comprise 85% of all water withdrawals (Maupin et al., 2014). Given the importance of the snowpack, water resource professionals and management agencies monitor the accumulation and storage patterns to forecast the volume (NRCS, 2012) and timing <www.cbrfc.noaa.gov> of snowmelt runoff. The resulting recommendations shape and inform decisions that allocate limited water resources across the western United States.

Data that accurately describe the snowpack characteristics are critical to management and monitoring efforts. The Natural Resource Conservation Service (NRCS) deploys and manages a network of automated snow telemetry (SNOTEL) stations to measure snowpack characteristics (snow water equivalent (SWE), precipitation, snow depth, and air temperature), with the goal of forecasting runoff volumes for rivers and streams across the mountainous western United States (NRCS, 2018). From the available data collected by the NRCS, scientists, researchers and water management professionals have developed methods and tools to replicate, model and/or forecast the aggregate volume, accumulation, ablation and runoff patterns of snowpack.

In the field of snowpack melt modeling, three distinct methods have been applied: linear-regression, temperature-index, and energy balance methods. Linear-regression techniques have been implemented to test correlation between SWE and total snowmelt runoff volume between April 1 and July 31 (Fassnacht, 2006), standard deviation and mean snow depth (Egli and Jonas, 2009), between peak SWE characteristics, and peak streamflow and annual runoff volume (Fassnacht et al., 2014). Temperature-index models apply empirical correlations between air temperatures and melt rates, and have been used to estimate the timing and quantity of peak streamflow (U.S. Army Corps of Engineers, 1956; Hock, 2003). In contrast, energy-balance models account for the cumulative impact of measurable environmental and thermodynamic processes on the snowpack, and relate the remaining residual energy to melt volumes and rates (Hock, 2003). In this paper, the empirical regression approach developed by Egli and Jonas (2009) was applied to investigate the hysteretic dynamics of seasonal snow distribution.

Egli and Jonas (2009) characterized the dynamics of spatio-temporal snow depth distribution for both accumulation and ablation phases based on six years of data from 77 weather stations across the Swiss Alps. They applied analytical methods originally developed in the field of statistical physics by Barabási and Stanley (1995) to describe snowpack depth as a growing then diminishing surface over time. To visualize and analyze snow depth and variability across the domain, Egli and Jonas (2009) adapted a statistical technique from Crow and Wood (1999) and Famiglietti et al. (2008)'s soil analyses to present snow depth distribution (standard deviation) as a function of mean snow depth. The technique allowed for the identification and parameterization of mean snow depth distributions for accumulation and ablation phases.

This study applied the assumptions and methods developed by Egli and Jonas (2009) for the Swiss Alps to the headwaters region in the Southern Rocky Mountains (SRM), considering several adaptations. Across the SRM region, there are different snow climatologies (Fassnacht and Derry, 2010), with large spatial and elevation variability, a longer period of record (Fassnacht and Records, 2015), but a lower spatial density of snow measurement stations compared to the Alps study. While Egli and Jonas (2009) used snow depth, this work focused on SWE due to the longer record of SWE data compared to snow depth (NRCS, 2018).

This work in the SRM region builds upon previous snow hydrology studies using the same dataset, in particular the derivation of snow-cover depletion curves (Fassnacht et al., 2016), the spatio-temporal variability of snowmelt factors (Fassnacht et al., 2017), the evaluation of snowmelt rates compared to precipitation as potential for flood risk (Fassnacht and Records, 2015), and snowmelt modeling (Ma, 2017; Ma et al., 2019). This paper examined 34 water years (Oct 1, 1981 – Sept 30, 2015) of SWE data across the Southern Rocky Mountains to (1) compare the hysteretic nature of snow depth and SWE standard deviation versus mean trajectories, (2) identify regression models and parameters to approximate the accumulation phase of SWE trajectories over the period of record, and (3) identify characteristics and patterns across the SRM by sub-dividing the domain by latitude, elevation and snow year magnitude.

2.0 STUDY AREA DATA

Snow water equivalent measurements are taken at over 800 Natural Resources Conservation Service (NRCS) Snow Telemetry (SNOTEL) stations across the western continental United States. There are 90 stations across the Southern Rocky Mountains study area that were used in this study (Figure 2-1). Stations within the study domain stretch from approximately 36 to 42.5 degrees North and 105 to 109 degrees West within the states of Colorado, northern New Mexico and southern Wyoming and across the elevation range of 2268 to 3536 meters (Figure 2-1). Mean daily SWE values recorded between water years 1982 and 2015 were obtained from the NRCS <wcc.nrc.usda.gov>. The available period of record for the stations was between 28 and 34 years. Quality-controlled SWE data were obtained from Fassnacht and Records (2015).

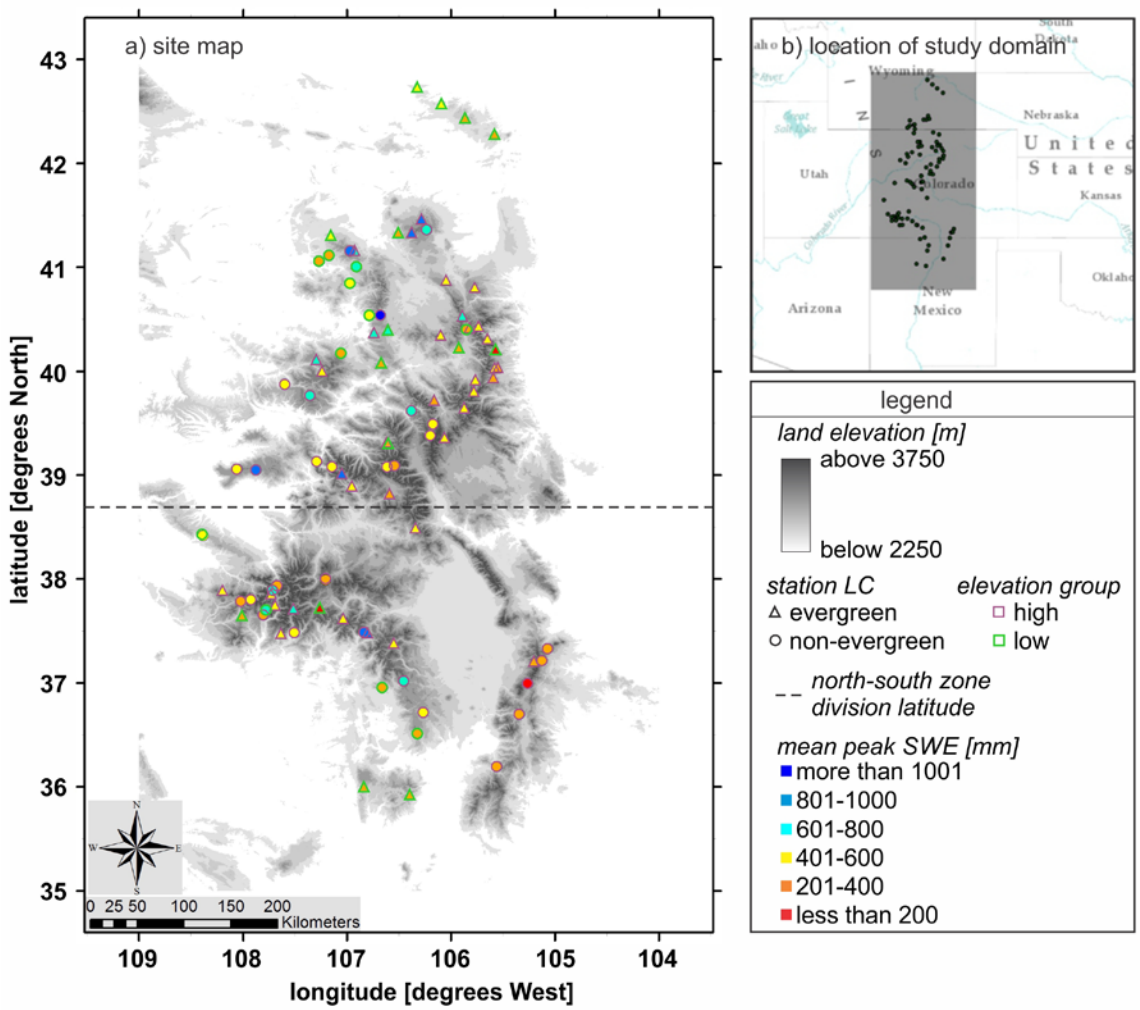

Figure 2-1. (a) Location, elevation group (high/low), land cover (evergreen/non-evergreen) and mean peak SWE (mm) of 90 SNOTEL stations across the Southern Rocky Mountains. (b) Location of study domain

3.0 METHODS

The Methods are separated into five sections (3.1-3.5). Each section has one purpose (Table 3-1) and describes one step in the analysis process.

Table 3-1. Outline of the methods and purpose of each section

Methods Section	Purpose
3.1	Segment SRM domain spatially and classify the snow years
3.2	Show derivation of standard deviation versus mean trajectory
3.3	Compare snow depth and SWE variables for use in trajectory
3.4	Develop regression model and parameters to describe accumulation phase of trajectory
3.5	Outline statistics and categories utilized to characterize results

3.1 CLASSIFICATION OF SNOTEL DATA BY LATITUDE, ELEVATION AND SNOW YEAR MAGNITUDE

Quality-controlled water year data yielded a 24-hour average SWE value for each calendar day for each of the 34 water years (e.g., water year 1982 is Oct 1, 1981 to Sept 30, 1982). Grouping the SWE values together allowed the daily mean SWE and standard deviation SWE to be computed. Three groups of daily station data were considered, based on latitude and elevation (Table 3-2), yielding a total of seven unique mean and standard deviation SWE values for each calendar day. The Latitude-based group divided the SNOTEL stations across the SRM at 38.75 degrees north latitude into north and south sub-sets, based on regions of homogeneity identified with self-organizing map analyses (Fassnacht and Derry, 2010) and correlogram analyses of accumulation slopes (Von Thaden, 2016). The Latitude- and elevation-based group further subdivided the north-south SNOTEL stations sub-sets by an elevation threshold of 2800 meters in the north and 2900 meters in the south. Elevation thresholds were selected to the nearest 100 meters, and to have a similar proportional distribution of low stations for the north and south sub-sets.

Table 3-2. Outline of the discretization of SNOTEL data within the Southern Rocky Mountains domain

Groups	**Sub-set**	**Number of Stations**
Summary	full domain	90
Latitude-based	North region	57
	South region	33
Latitude and Elevation-based	North region & High elevation	39
	North region & Low elevation	18
	South region & High elevation	25
	South region & Low elevation	8

For each spatial sub-set, all 34 snow years were classified according to the annual maximum daily SWE measurement. Three classifications were developed: above average (AA), average (AVG) or below average (BA). Snow years with an annual maximum daily

SWE within (±) one standard deviation of the 34-year average were classified as AVG, while snow years with an annual maximum daily SWE value below the lower bound were classified as BA, and snow years with an annual maximum daily SWE above the upper bound were classified as AA.

3.2 DERIVATION OF SWE STANDARD DEVIATION VERSUS MEAN TRAJECTORIES

For each station (i) in the study domain, and day (t) in the snow year, the 24-hour average SWE value is represented by $x_i(t)$. Averaging these values across a single sub-set yields, $\overline{x_\iota(t)}$, or the mean daily SWE. For each sub-set of mean SWE values, the daily standard deviation $\sigma(x_i, t)$ was obtained as follows (Egli and Jonas, 2009):

$$\sigma(x_i, t) = \sqrt{\frac{1}{N-1}\sum_{i=1}^{N}[\, x_i(t) - \overline{x_\iota(t)}]^2} \qquad (1).$$

Thus, for each calendar day (t) between 1982 and 2015, and each sub-set of SNOTEL stations (i), the mean and standard deviation SWE were developed. Seven sub-sets were analyzed over the 34-year period of record, yielding 238 unique instances (Table 3-1).

Egli and Jonas (2009) utilized this methodology "*to describe the evolution of the snow cover as a growing surface*," based on prior work by Barabási and Stanley (1995) and Löwe et. al. (2007). When the snow cover ($\overline{x_\iota(t)}$, SWE) is considered to be a growing/diminishing surface across the snow year, the standard deviation $\sigma(x_i, t)$ within the data set reflects the magnitude of spatial variability. This paper utilized one additional technique adopted by Egli and Jonas (2009); plotting standard deviation $\sigma(x_i, t)$ as a dependent function of mean $\overline{x_\iota(t)}$. The approach enabled the seasonal SWE distribution (or snow depth, as used by Egli and Jonas, 2009) to be modeled across multiple spatio-temporal scales, independent of time. As a result, a unique standard deviation SWE value was correlated to each mean SWE value.

3.3 EVALUATION OF SWE AND SNOW DEPTH AS VARIABLES FOR THE STANDARD DEVIATION VERSUS MEAN TRAJECTORY

Prior accumulation and ablation trajectory analyses by Egli and Jonas (2009) considered snow depth rather than SWE data. SWE data were selected because the data were available for a longer period of record, and at a higher spatial density than snow depth in the SRM. Both SWE and snow depth data were evaluated to compare accumulation phase regression statistics and slope coefficients between SWE and snow depth trajectories. One snow year from each snow year magnitude category in the full domain sub-set was selected: 2012 from the BA category, 2010 from the AVG category, 2011 from the AA category. For all three snow years, the daily standard deviation data over 90 (87) SWE (snow depth) stations across the full domain were plotted against the daily mean over all 90 (87) stations to develop both snow depth and SWE trajectories. The inflection point between accumulation and hysteresis periods was identified visually and used as an upper bound for regression

models. Linear regression equations were developed, regression statistics (slope coefficients, coefficient of determination values) were extracted, and differences between the regression data were evaluated.

3.4 DEVELOPMENT OF ACCUMULATION TRAJECTORY MODELS

To characterize and describe snowpack as a singular growing surface, both the regression model (e.g. linear, power) and inflection point parameters (e.g. slope threshold) were investigated. Standard deviation versus mean trajectories from seven characteristic snow years in the full domain sub-set were evaluated to identify the optimal regression model and inflection point parameters. Of the seven characteristic snow years, one to three year(s) of data were obtained from each snow year magnitude category to represent BA (2002, 2012, 2013), AVG (2010) and AA (1993, 1995, 2011) snow years (Figure 3-1). Snow years were selected based on the presence or absence of distinct trajectory characteristics, such as the curvature and shape of the transition between accumulation, hysteresis and ablation phases, and the relationship between the maximum standard deviation SWE and maximum mean SWE. Special consideration was given to select trajectories with distinct behavior.

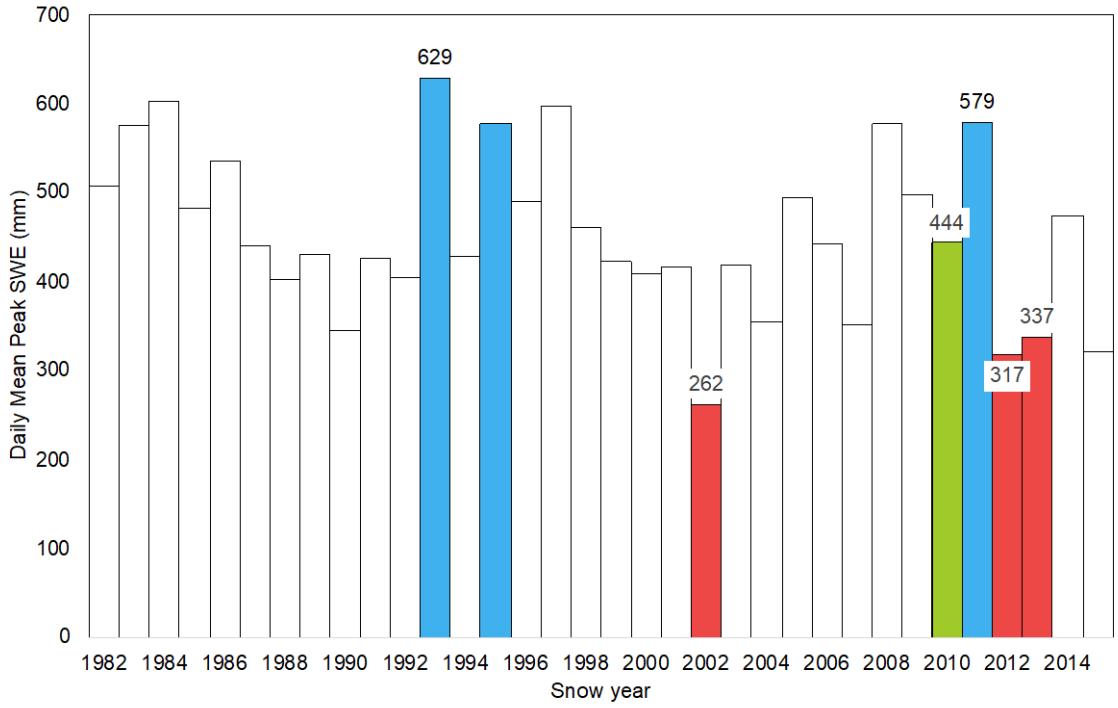

Figure 3-1. Daily mean peak SWE (cm) in the full domain (AA = blue, AVG = green, BA = red), with seven characteristic years bolded and labeled.

Similar to Egli and Jonas (2009), a sensitivity analysis was conducted to identify parameters that enable detection of the accumulation phase inflection point (Figure 3-2). A moving-slope difference approach was used, and three different variables were tested: indicator position, magnitude difference in slope, and last feasible calendar date that all stations could be in accumulation phase. For every data point (day) in the domain, linear

regression variables were calculated based on the adjacent data points to determine the 10-day or 11-day average accumulation slope. A 10-day linear regression was conducted for the leading (9 days prior, present day), and lagging (present day, future 9 days) indicator positions, and an 11-day linear regression was conducted for the central indicator position (5 days prior, present day and future 5 days). The difference in slopes between consecutive days was calculated, and slope difference thresholds of 0.3 and 0.5 were tested. Large differences in slope were assumed to correlate with the end of the quasi-linear accumulation phase. Multiple dates for the feasible calendar date for all stations to be in accumulation phase was also tested. The feasible calendar date was included to maintain data quality.

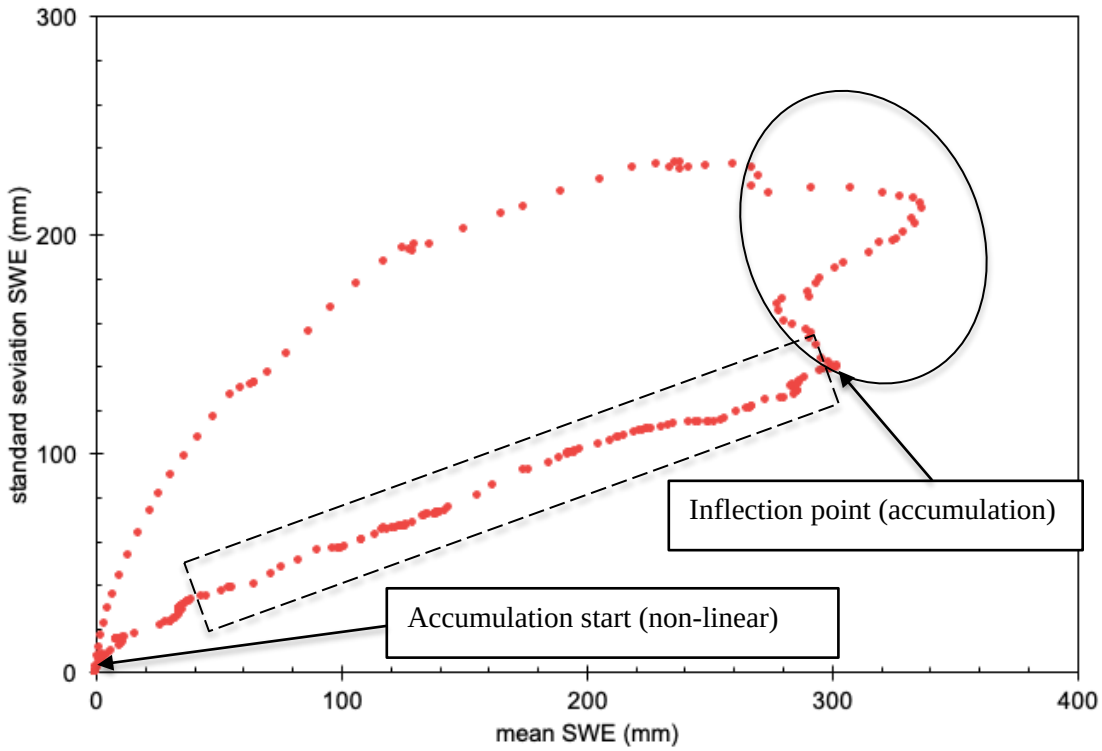

Figure 3-2. Sample standard deviation versus mean SWE trajectory (full domain, 2013), with accumulation start (non-linear) and the accumulation inflection point identified. The approximate accumulation phase (square, dashed lines) and hysteresis phase (oval, solid line) are included.

Inflection points obtained from all six permutations of slope difference threshold and indicator position variables were compared to the ideal inflection point, which was identified by visual inspection for the seven characteristic snow years. The Nash-Sutcliffe coefficient of efficiency (NSCE) was calculated to measure the ability of each set of model parameters to replicate the ideal inflection point. Linear regression was applied to the observed ideal inflection point versus the modeled inflection point, and the coefficient of determination was calculated.

After the optimal inflection point parameters were identified, three regression methods were applied to the same seven years' standard deviation versus mean SWE domain data. Linear (2) and truncated linear (3), and power (4), regression models were considered, based on prior work by Egli and Jonas (2009) and Pomeroy et al. (2004). For both the linear and power regressions, the entire accumulation data set from initial non-zero values through the inflection point were considered, and coefficients M and B and α and β were identified by the following equations:

$$\sigma(x_i, t) = \mathrm{M} \times \overline{x_\iota(t)} + \mathrm{B} \qquad (2, 3), \text{ and}$$

$$\sigma(x_i, t) = \alpha \times \overline{x_\iota(t)}^{\beta} \qquad (4).$$

A truncated linear regression model was developed specifically to exclude SWE data from the beginning of the accumulation phase, characterized by non-linear patterns and significant moving-average slope variability. The non-zero initial point (first occurrence of mean SWE ≥ 35 mm) was selected by reviewing the standard deviation versus mean SWE trajectories trends visible on all seven characteristic years, with a focus to exclude the initial non-linear snowfall accumulation phase (Figure 3-2).

3.5 METHODS TO EVALUATE ACCUMULATION TRAJECTORIES AND BEST-FIT MODELS

After the ideal regression model and parameters were identified, both were applied to the accumulation phase of 238 standard deviation versus mean SWE trajectories (one trajectory per year in seven sub-sets (Table 3-2)). The iterative analysis was conducted with Python code, leveraging SciPy (Virtanen, et al. 2020) and pandas (McKinney, 2010) packages. For each trajectory, slope and coefficient of determination regression statistics were obtained. Within each sub-set, maximum, minimum, average and standard deviation statistics based on the 34 slope values were calculated and each snow year was identified as BA, AVG and AA. The upper and lower boundaries used to categorize the snow year were developed uniquely for each sub-set as described in Section 3-3 based on mean and standard deviation of the sub-set.

4.0 RESULTS

4.1 EVALUATION OF SWE AND SNOW DEPTH STANDARD DEVIATION VERSUS MEAN TRAJECTORIES

The standard deviation versus mean snow depth and SWE trajectories for the three characteristic snow years have similar shapes (Figure 4-1). Within the accumulation phase, the trajectory can be broken into two distinct sections for both SWE and snow depth: a non-linear, hysteretic section for low mean snow depth/SWE values (typically less than 35 mm mean SWE), and a linear section with a positive average slope (Figure 4-1). Snow depth values have a higher degree of scatter along the trajectory than SWE (Figure 4-1). The degree of scatter is reflected in the regression statistics; coefficient of determination values for SWE are consistently close to 1 (linear), while coefficient of determination values for snow depth values are consistently lower (Table 4-1). Snow depth trajectories exhibit abrupt changes in the magnitude and direction of slope that are not seen for SWE during the accumulation phase. The linear accumulation slopes for SWE were greater than snow depth by 24% in 2010 and 2012, and 31% in 2011 (Table 4-1).

Table 4-1 – Comparison of linear regression slope and coefficient of determination for SWE (90 stations) and snow depth (87 stations)

Snow year	**Slope**		**Coefficient of determination**	
	SWE	**Snow Depth**	**SWE**	**Snow Depth**
2010	0.36	0.29	0.98	0.95
2011	0.49	0.38	0.99	0.97
2012	0.36	0.29	0.98	0.95

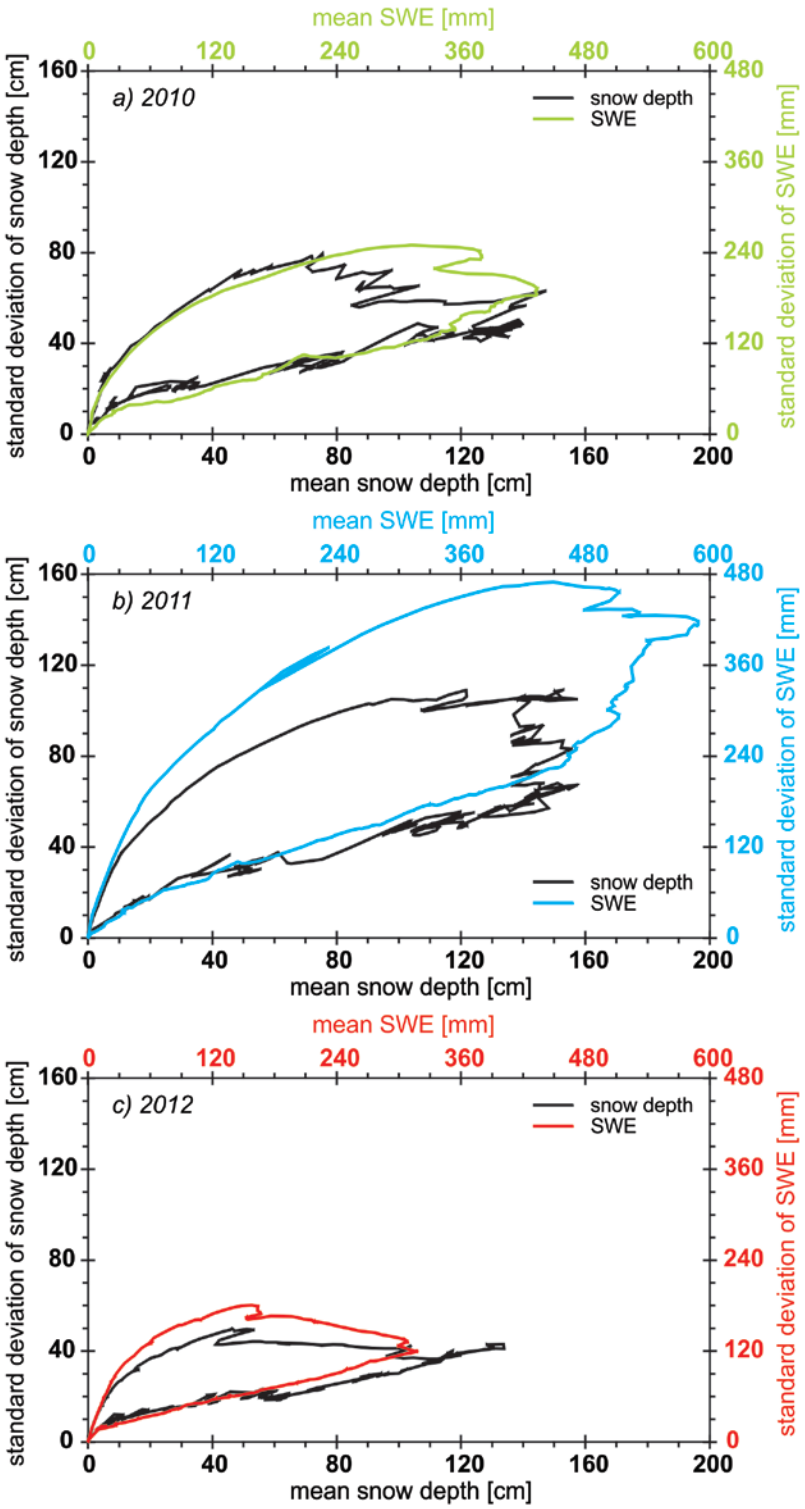

Figure 4-1. Mean and standard deviation of mean daily data for snow depth (87 SNOTEL stations) and SWE (90 SNOTEL stations) for the 2010 (top, green), 2011 (middle, blue) and 2012 (bottom, red) snow years.

4.2 IDENTIFICATION OF THE OPTIMAL ACCUMULATION TRAJECTORY MODEL AND PARAMETERS

The linear, truncated linear, and power regression models each fit the measured accumulation phase data (seven characteristic years, full domain (Figure 4-2)) very effectively. Coefficient of determination values are reported to three decimal places to differentiate the fit (Table 4-2). The coefficient of determination values for the two linear models are closer to a perfect fit (1) than for the power function. By excluding SWE data below 35mm, the linear model the fit improves, and the average coefficient of determination is 0.994 for the seven characteristic years.

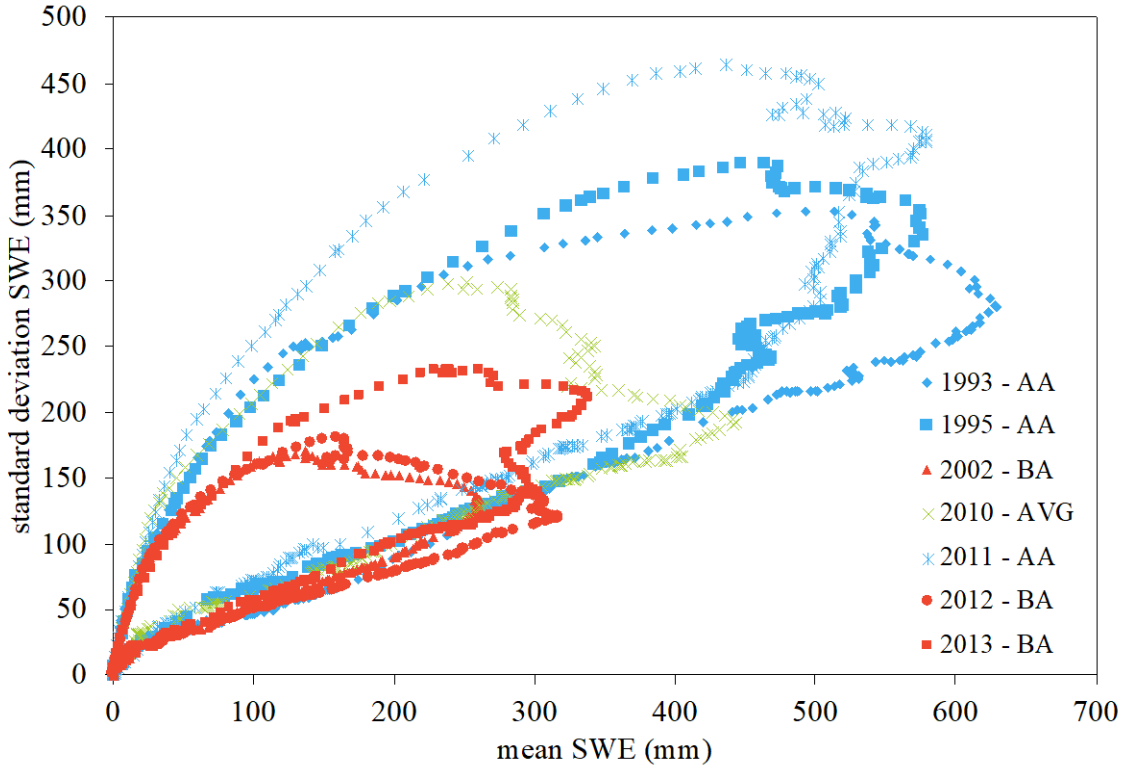

Figure 4-2. Standard deviation versus mean SWE trajectory data (full domain) from seven characteristic snow years that were used to define accumulation inflection point and regression model.

Table 4-2 – Comparison of coefficient of determination values from three accumulation phase regression models for the seven study years (full domain) (see Figure 4-1).

Snow year	Linear	Truncated Linear at 35mm	Power
1993	0.998	0.997	0.983
1995	0.980	0.991	0.959
2002	0.986	0.989	0.986
2010	0.977	0.994	0.984
2011	0.987	0.997	0.995
2012	0.980	0.997	0.971
2013	0.987	0.995	0.991
Average	0.985	0.994	0.981

The slope difference threshold value of 0.5 did not lead to detection of an inflection point for the 2010 snow year (AVG), influencing the negative NSCE and low coefficient of determination values for linear regression between observed and modeled inflection points (Table 4-3). In contrast, the slope difference threshold of 0.3 led to the detection of an inflection point for all seven years. With a slope difference threshold value of 0.3, both the central 11-day and lagging 10-day indicator position parameters reflected the observed inflection point (NSCE of 0.85, 0.81 respectively), and exhibited a more linear relationship between observed and modeled mean SWE (coefficient of determination of 0.86, 0.87 respectively), than the leading 10-day indicator position parameter. The central 11-day (0.3 slope difference threshold) was utilized in regression model identification and results assessment, because this combination of parameters yielded the most accurate results for the seven characteristic snow years.

Table 4-3 – Accumulation phase inflection point model parameter comparison

Slope Difference Threshold	Indicator Position	NSCE	Coefficient of Determination
0.3	**leading 10-day**	0.71	0.76
	central 11-day	0.85	0.86
	lagging 10-day	0.81	0.87
0.5	**leading 10-day**	-1.97	0.01
	central 11-day	-0.31	0.55
	lagging 10-day	-0.42	0.44

4.3 EVALUATION OF ACCUMULATION TRAJECTORIES AND BEST-FIT MODELS

Out of the 238 trajectories, the model did not yield an inflection point or a realistic inflection point for nine years (3.7% of the trajectories): full domain – 2000, south – 2000, 2012, north-high – 1984, 2001, south-high – 1987, 2000, south-low – 2000, 2008. For these cases, the inflection point was obtained by visual inspection. Realistic inflection points were assumed to occur prior to May 15th.

The 34-year average of SWE accumulation slopes across all seven sub-sets range from 0.36 (south low) to 0.40 (full domain) (Table 4-4). The maximum slope was observed in the full domain sub-set in 2006 (slope = 0.59), and the minimum slope was observed in the south low elevation sub-set in 2007 (slope = 0.12). Across the four latitude and elevation based sub-sets, a slight decreasing trend in average slope was observed (0.01 change per sub-set), from highest and northernmost (north high = 0.39) to lowest and southernmost (south low = 0.36). However, average slopes were fairly consistent across all seven sub-sets. The largest range between maximum and minimum slopes was observed in the south-low sub-set (0.40), while the smallest range was observed in the north sub-set (0.18).

The 34-year average coefficient of determination (R^2) and standard deviation values were employed to assess the degree of inter-annual variability (or scatter) on the accumulation phase of the standard deviation versus mean SWE trajectories (Table 4-4). The south low sub-set exhibits a high degree of scatter (Figure 4-3) and had the lowest coefficient of determination (0.95), and highest slope standard deviation (0.097) of the slopes across all sub-sets. Conversely, the north and north low sub-sets exhibited the highest coefficient of determination (0.99), but the north sub-set exhibited the lowest variation (slope standard deviation of 0.042).

Table 4-4 – Summary of accumulation phase data

		Slope Statistics obtained from 34 years of results				
Group	**Sub-set**	**Average slope**	**Max slope**	**Min slope**	**Average slope R^2**	**Slope standard deviation**
Summary	Full domain	0.40	0.59	0.26	0.98	0.062
Latitude-based	North	0.39	0.47	0.29	0.99	0.042
	South	0.37	0.50	0.23	0.97	0.077
Latitude and Elevation-based	North High	0.39	0.49	0.28	0.98	0.053
	North Low	0.38	0.47	0.26	0.99	0.049
	South High	0.37	0.57	0.23	0.97	0.083
	South Low	0.36	0.52	0.12	0.95	0.097

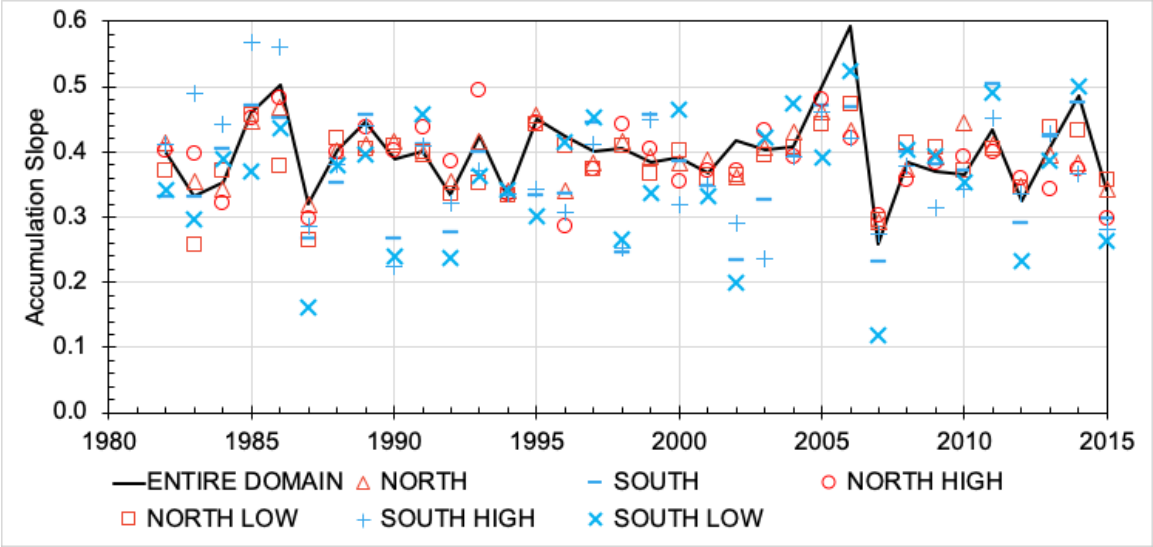

Figure 4-3. Average accumulation slopes per year for all sub-sets illustrate the inter-annual variability of standard deviation versus mean trajectories.

Little to no correlation between scatter and elevation was observed, since separating the south and north sub-sets by elevation into high and low sub-sets yielded equal or slightly lower (0.01-0.02) coefficient of determination values. Conversely, the magnitude of scatter and elevation appear to be correlated, because separating the south and north sub-sets by elevation into high and low sub-sets increased the standard deviation for all four sub-sets. The largest increase in standard deviation was observed in the south low sub-set, as standard deviation increased 0.020 (from 0.077 (south) to 0.097 (south low)), while the increase in standard deviation for the other three sub-sets was observed between 0.006 (south to south high) and 0.011 (north to north high).

When the accumulation phase data are discretized by snow year magnitude (BA, AVG, AA) and sub-set, several characteristics become apparent (Figure 4-4). Generally, below average (BA) snow years exhibited lower average accumulation slopes than average (AVG) or above average (AA) snow years (six out of seven sub-sets); the lowest average accumulation slope – regardless of snow year – was observed in the south high region in the BA snow year category. The standard deviation values were fairly similar within each sub-set, except the south low sub-set where accumulation slopes were much more variable in BA snow years than AVG or AA snow years.

Between the north- and south sub-sets, the average accumulation slopes for BA and AA snow years were fairly consistent, but a large difference in average accumulation slope was observed for AVG snow years. When elevation was considered in the north sub-set (splitting into north high and north low sub-sets), no significant impact from snow year category was observed, since the average slope and standard deviation values were fairly consistent. However, when elevation was considered in the south sub-set (south high and south low), significant fluctuations in average slope and standard deviation were observed. For example, average slopes for BA snow years decreased, AVG snow years increased, and AA snow years both increased (high elevation) and decreased (low elevation). Discretizing the south sub-set data by elevation revealed standard deviation (scatter)

increased for all snow years and both elevation sub-sets, except BA snow years in the south-high sub-set.

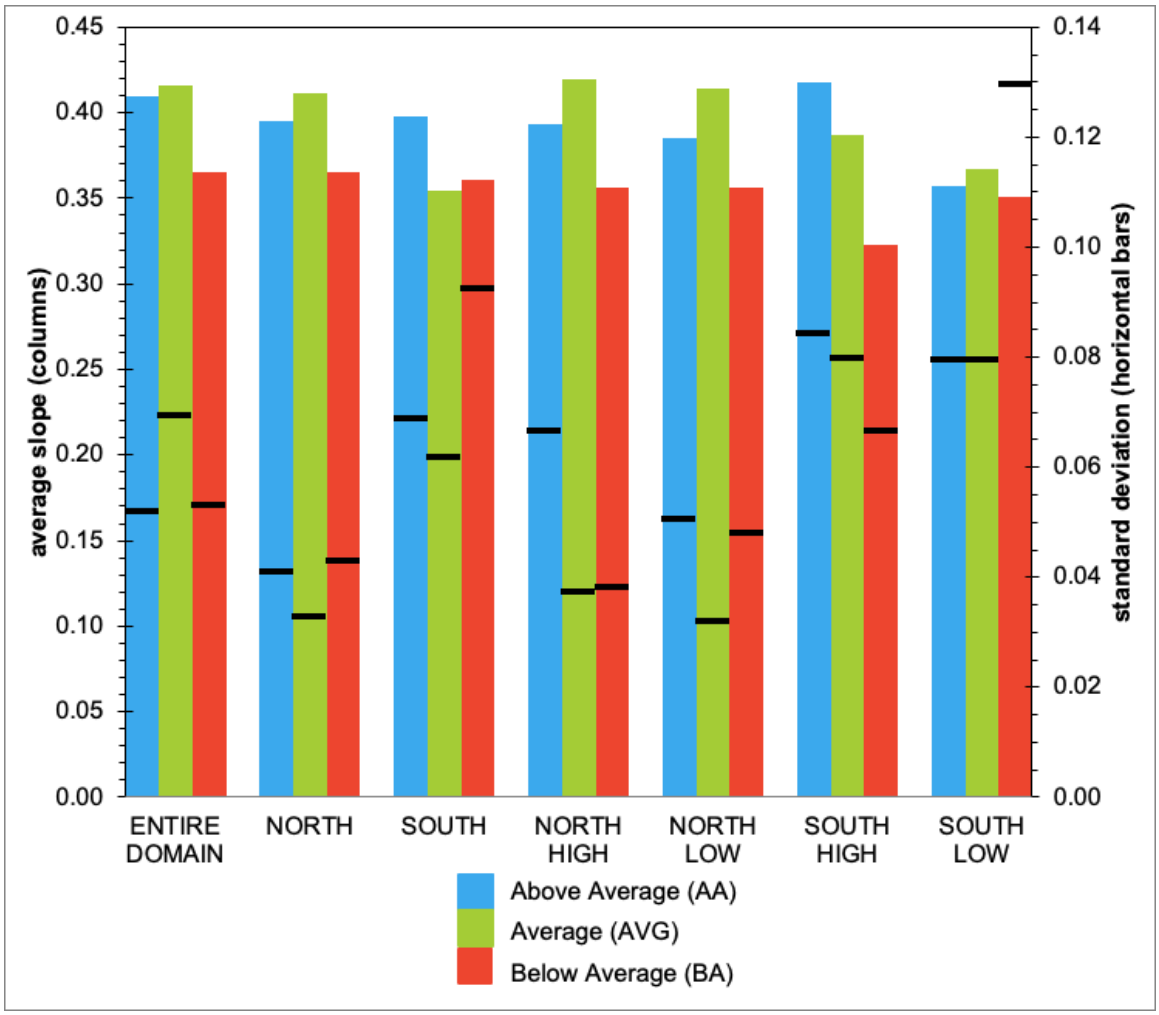

Figure 4-4. The 34-year average accumulation slopes and standard deviation separated by peak annual daily SWE (BA, AVG and AA snow year magnitude categories) are presented across seven sub-sets based on elevation and latitude.

The largest difference in average accumulation slope within a sub-set was observed in the south high sub-set, where the range between the largest (AA snow year = 0.42) and smallest (BA snow year = 0.32) average slopes was 0.10. The smallest difference in average accumulation slope within a sub-set was observed in the south low sub-set, with a range of 0.02, between AVG (0.37) and BA (0.35) snow years. The extreme range between the largest and smallest accumulation slopes in south low and south high sub-sets were in contrast to the ranges observed in the other five sub-sets, between 0.04 and 0.06. Collectively, the results suggest that average accumulation slope values are correlated strongly, moderately, or weakly with the peak annual SWE; south low = little to no correlation, south high = strong correlation, other five sub-sets = moderate correlation. Stated differently, average accumulation values are fairly consistent for the south low sub-set, regardless of snow year. Conversely, for the south high sub-set, average accumulation

slopes vary greatly, based on the snow year. For the remainder of the sub-sets, accumulation slopes vary to a moderate extent, based on the snow year.

5.0 DISCUSSION

5.1 APPLICABILITY OF SWE AND SNOW DEPTH DATA FOR STANDARD DEVIATION VERSUS MEAN TRAJECTORIES

An initial objective of this study was to assess whether SWE could be substituted for snow depth in the trajectory, since prior work by Egli and Jonas (2009) utilized snow depth data. The use of SWE instead of snow depth data was motivated by robustness of the available data. In the SRM, SWE data are available for longer period of record and greater spatial extent than snow depth data. A second motivation was variability in the trajectory data identified by Egli and Jonas (2009).

Results from Section 4.1 suggest that SWE data are a good substitute for and provide several advantages over snow depth data. For the three snow years where regression was applied to snow depth and SWE data (2010, 2011, 2012), the coefficient of determination values were closer to 1 for SWE data (Table 4-1). The regression fit parameters confirm visual observations from the trajectories (Figure 4-1); the standard deviation varies less with SWE data than with snow depth data. In the accumulation phase, snow depth data lead to a trajectory with multiple standard deviation values for a given SWE value, which was not observed for trajectories based on SWE data (Figure 4-1). Egli and Jonas (2009) observed the same behavior – high variability and frequent changes in snow depth standard deviation. Egli and Jonas (2009) attributed this behavior to physical processes of settling and/or densification, which are measured by snow depth. The SWE trajectory does not exhibit abrupt changes in magnitude/direction or multiple values of standard deviation for a given SWE value, because SWE measures the mass of accumulated water rather than snow depth and decreases in SWE are smaller due to sublimation. The SWE trajectories generally do not exhibit decreases in mean SWE until the start of ablation phase, because mid-winter (accumulation phase) melt events are rare across the SRM (Fassnacht and Patterson, 2013). The use of SWE data eliminated variability due to physical processes of settling and densification (Figure 4-2), resulting in an accumulation trajectory to which regression can be applied with greater accuracy than snow depth data (Table 4-1).

5.2 REVIEW OF REGRESSION MODEL AND PARAMETERS APPLIED TO SWE TRAJECTORY

Although the original work on growing surfaces by Barabási and Stanley (1995) and Egli and Jonas (2009) elected to model the accumulation phase of the trajectory with a power function, the truncated linear model most accurately fit the accumulation phase in the SRM. For the seven characteristic years in the full domain sub-set, the truncated linear model yielded a coefficient of determination equal to, or greater than the linear or power models (Table 4-2). However, all three models yielded high coefficient of determination values, confirming prior findings by Egli and Jonas (2009) and Pomeroy et al. (2004) that both power and linear models can be applied to the accumulation phase across different snow measurement variables (snow depth/SWE) and snow hydrology regions (SRM, Swiss Alps).

The truncated linear regression model improves the fit over the non-truncated linear model by excluding mean SWE values below 35 mm from the regression. For all seven years analyzed in depth, the trajectory data below 35 mm were highly variable and had multiple standard deviation values for a given SWE value. The 35 mm threshold was selected to eliminate the majority of the variability and duplicate standard deviation values by visual analysis from the seven snow year trajectories studied in depth (Figure 4-2). This driver of this behavior is likely caused by both individual SNOTEL stations shifting from accumulation to ablation, and the 90-station aggregate including stations in both accumulation and ablation phases at the onset of the winter season. Similar behavior can be observed during the hysteresis period between purely accumulation and ablation phases (Figure 4-2).

Whether generated from snow depth or SWE data, average accumulation slope values are a measure of spatial variability; larger slope values indicate snowpack data are more heterogenous, while lower slopes indicate snowpack data are more homogenous. Both SWE and snow depth accumulation slopes in the SRM were generally lower than the linear regression slopes for snow depth observed by Egli and Jonas (2009) in the Swiss Alps. In the SRM, snow depth accumulation slopes ranged from 0.29 to 0.38 (the average over 2010, 2011, 2012 was 0.32), and 34-year average SWE accumulation slopes ranged 0.36 (south low sub-set) to 0.40 (full domain) (Table 4-4). Egli and Jonas (2009) reported six-year average accumulation slopes between 0.41 and 0.54. Physical processes, such as snow settling, account for the difference in slope between snow depth and SWE data, but do not account for the difference in snow depth slope observed between the SRM and Swiss Alps.

The smaller accumulation slopes in the SRM could be due to differences in data density, period of record analyzed, or snowpack climatology. Egli and Jonas (2009) utilized data from 77 stations located over approximately 30,000 km^2 (390 km^2/station), while this study utilized data from 90 stations spread out over approximately 300,000 km^2 (3,330 km^2/station). Differences in snow hydrology between the Swiss Alps and SRM may contribute as well. For example, the annual peak station-averaged snow depth observed by Egli and Jonas (2009) in the Swiss Alps was between 1.53-2.42 meters, while the annual peak station-average snow depth in the SRM was between 0.75-3.0 meters <wcc.nrcs.usda.gov>. The period of record Egli and Jonas (2009) considered was for six snow years with some variability. In this paper, three years of snow depth data illustrated larger inter-annual variability (Figure 4-1). In total, 34 years of SWE were considered for the SRM, illustrating much variability (Table 4-4, Figure 4-3). Finally, the SRM domain in this paper is an order of magnitude larger than the Swiss Alps region examined by Egli and Jonas (2009). As such, there is much difference in snowpack accumulation patterns across the SRM (Von Thaden, 2016) that are not seen in the Swiss Alps study domain. These differences across the SRM (Fassnacht and Derry, 2010) are especially pronounced between the northern and southern portions of the area (Figure 2-1). The SRM domain is large enough (>700 km north to south) that snowfall usually arrives from different storm systems across the domain.

5.3 DISCUSSION OF OBSERVED ACCUMULATION SLOPE DYNAMICS IN THE SRM

The 34-year average accumulation slopes of standard deviation versus mean trajectories illustrate that similar snowpack accumulation patterns exist across the SRM, which has previously been detailed by Sturm and Wagner (2010). Unique snowpack accumulation patterns were observed across the distinct snow climatologies of the SRM previously identified and characterized by Fassnacht and Derry (2010). The snowpack in the south region was slightly more spatially homogenous than in the north region for individual years, because the 34-year average accumulation slope is lower in the south region than in the north. However, the higher standard deviation for the 34-year average accumulation slope in the south region indicated more inter-annual variability of the snow surface than in the north region.

The most numerically significant impact of elevation was observed when the north and south sub-sets were split into high and low sub-sets, because the 34-year average standard deviation values increased for all elevation and latitude-based sub-sets. While the relatively small number of data points within the twice-divided sub-sets may account for a portion of this change, the results may also suggest substantial snowpack variability exists across sites within similar elevation and latitude ranges. However, the accumulation slopes from the same elevation- and latitude-based sub-sets are very similar to the latitude-based sub-sets. Consistency in the average accumulation slope between elevation- and non-elevation based sub-sets suggests that for larger spatial scales and data sets, elevation does not dramatically impact spatial or inter-annual snowpack accumulation patterns.

When annual maximum daily SWE for each snow year is discretized into BA, AVG and AA snow years, clear correlations between slope, peak annual SWE, elevation and latitude were observed across the 34-year accumulation phase trajectories. Average accumulation slopes differ somewhat for BA, AVG and AA snow years for the north sub-set, and those differences are amplified in the north high and north low sub-sets. The consistency suggests that distinct snowpack accumulation patterns exist for different annual maximum SWE categories, and that elevation does not impact snowpack accumulation behavior. BA snow years exhibit the lowest average slope, corresponding to the lowest degree of spatial heterogeneity, followed by AA snow years, and then AVG snow years with the highest degree of spatial snowpack variability. Within the south low region, consistency in average accumulation slope across BA, AVG and AA snow years suggests peak annual SWE has no impact on the spatial distribution of SWE. However, the large range of standard deviation values in the south low sub-set reflects a unique characteristic of BA peak SWE snow years; a high degree of spatial variability in snowpack.

5.4 FUTURE WORK RELATED TO SWE TRAJECTORIES

This paper successfully applied many of Egli and Jonas (2009) methods and assumptions to the SRM snow climatology, compared snow depth and SWE trajectories, and modeled the accumulation phase of the SWE standard deviation versus mean trajectory, but a number of additional perspectives could be considered in future work. The ablation phase

and hysteretic transition period between accumulation and ablation should be characterized and modeled similarly. A complete model of accumulation and ablation would represent the entire cycle of seasonal snowpack and provide insight on the potential relations between elevation, latitude and snow year on snowpack as a diminishing surface. Although Egli and Jonas (2009) hypothesis regarding increased heterogeneity at the initiation of ablation phase was visually observed and additional studies may be able to characterize and quantify this phenomenon. Within the same period of record, statistical tests could be applied to trajectory characteristics to investigate potential temporal trends, patterns or markers of non-stationarity. Additional work could include analyses to test for correlation between trajectory characteristics (i.e. slope, breakpoint) and external global climatic patterns, such as drought indices or the Oceanic Niño Index (ONI).

6.0 CONCLUSIONS

This study attempts to characterize and visualize the annual growth of snowpack in the Southern Rocky Mountains with a graphically-based trajectory methodology. For a given spatial domain, daily mean/standard deviation measurements of snowpack were applied to a linear plot, illustrating three phases of snowpack evolution: accumulation, ablation and mixed accumulation and ablation. Snow depth and snow water equivalent data from 90 SNOTEL stations from 34 water years (1981-2015) were used to answer several questions: can snow depth and SWE be used to describe annual snowpack evolution in the Southern Rocky Mountains?, what regression models and parameters describe the accumulation phase trajectory?, and when the SWE data are divided by elevation, latitude and snow year magnitude, do any characteristics or patterns emerge?

To characterize differences between snow depth and SWE data, trajectories for three years (2010-2012) in the full domain sub-set were developed, and linear regression was applied to the accumulation phase. Linear accumulation slopes for SWE were greater than snow depth by 24% in 2010 and 2012, and 31% in 2011, and multiple values of standard deviation for a given mean value were more likely on the snow depth trajectory. This hysteretic behavior was attributed to snow depth capturing the physical processes of settling. Snow water equivalent data did not exhibit the same behavior and do not measure these physical processes.

Snow depth accumulation slopes for three years (2010, 2011, 2012) in the SRM were compared to accumulation slope values developed by Egli and Jonas (2009) in the Swiss Alps. Slopes in the SRM were lower than in the Swiss Alps. Data density (3,330 km^2/station in SRM, 330 km^2/station in Swiss Alps) and average peak snow depth (0.7 to 3.0 m in the SRM, 1.53 – 2.40 m in Swiss Alps) are plausible explanations for these differences.

Seven characteristic snow years (1993, 1995, 2002, 2010-2013) were selected to identify a regression model (linear, truncated linear, and power) and boundary condition parameters to detect the end of the accumulation phase and the beginning of mixed accumulation and ablation phases. The seven years were selected from the full domain sub-set with a distribution of snow year magnitude values (3 below average (BA), 1 average (AVG), and 3 above average (AA)), and unique trajectory characteristics. The seven-year average coefficient of determination for linear and power models were equal (0.98). Eliminating the initial hysteretic period (mean SWE < 35mm) from the linear model yielded a coefficient of determination = 0.99. Using the slope difference method, an 11-day moving average and slope difference threshold of 0.3 most accurately predicted the end of accumulation phase, compared to visual observation. The truncated linear model and slope difference parameters were used to analyze the accumulation slopes for 238 trajectories, based on all combinations of latitude (north/south split by 38.75 degrees north), elevation (high/low split by 2800 m (north) and 2900 m (south)) and snow year (above/below/within one standard deviation from the mean annual peak SWE).

Across all seven sub-sets the 34-year average accumulation slopes ranged from 0.36 (south low) to 0.40 (full domain), with 1-year slope values ranging from 0.59 (2006, full domain) to 0.12 (2007, south low). The 34-year average slope standard deviation values were lowest for the north (0.42) subset and highest in the south low (0.97) subset. The results suggest latitude influences snowpack variability: north of 38.75 degrees (north-based subsets) there is less interannual variability (south-based sub-sets) and south of 38.75 degrees there is more variability, especially below elevation 2900 m.

For all sub-sets BA snow years exhibited lower average accumulation slopes than AA snow years, suggesting snowpack variability is positively correlated with maximum annual peak SWE. South of 38.75 degrees and above 2900 meters (south high sub-set), AA snow years (average slope = 0.42) yield less variability in snowpack, and BA snow years (average slope = 0.32) exhibit substantial variability in snowpack. Perhaps unexpectedly, in the south low sub-set, average slope values are nearly identical for AA (0.36), AVG (0.36) and BA (0.35) snow years. Within the south low sub-set, a high degree of interannual variability in snowpack was noted (average accumulation slope standard deviation = 0.13).

From a relative perspective (minor/moderate/major), the study results suggest snowpack variability is influenced by elevation (moderate and dependent on latitude and snow year combination), latitude (moderate), and snow year (minor).

LITERATURE CITED

Barabási, A.L., and Stanley, H.E., 1995. Fractal Concepts in Surface Growth: Cambridge, U.K., Cambridge University Press.

Crow, W.T., and Wood, E.F., 1999. Multi-scale dynamics of soil moisture variability observed during SGP97. Geophysical Research Letters 26, 23, 3485-3488, doi:10.1029/1999GL010880.

Egli, L., and Jonas, T., 2009. Hysteretic dynamics of seasonal snow depth distribution in the Swiss Alps. Geophysical Research Letters 36, L02501, doi:10.1029/2008GL035545.

Famiglietti, J.S., Ryu, D., Berg, A.A., Rodell, M., and Jackson, T.J. 2008. Field observations of soil moisture variability across scales, Water Resources Research, 44, W01423, doi:10.1029/2006WR005804.

Fassnacht, S.R., 2006. Upper versus lower Colorado River sub-basin streamflow: characteristics, runoff estimation and model simulation, 2006. Hydrological Processes, 20, 2187-2205, doi: 10.1002/hyp.6202.

Fassnacht, S.R., Deitemeyer, D.C., Venable, N.B.H., 2014. Capitalizing on the daily time step of snow telemetry data to model the snowmelt components of the hydrograph for small watersheds, 2014. Hydrological Processes 28: 4654-4668, doi:10.1002/hyp.10260

Fassnacht, S.R., and Records, R.M., 2015. Large snowmelt versus rainfall events in the mountains, Journal of Geophysical Research: Atmospheres, 120, 2375-2381, doi:10.1002/2014JD022753.

Fassnacht, S.R., López-Moreno, J.I., Ma, C., Weber, A.N., Pfohl, A.K.D., Kampf, S.K., Kappas, M., 2017. Spatio-temporal snowmelt variability across the headwaters of the Southern Rocky Mountains, Frontiers of Earth Science, 11, 505-514, doi:10.1007/S11707-017-0641-4.

Fassnacht, S.R., Sexstone, G.A., Kashipazha, A.H., López-Moreno, J.I., Jasinski, M.F., Kampf, S.K., Von Thaden, B.C., 2016. Deriving snow-cover depletion curves for different spatial scales from remote sensing and snow telemetry data. Hydrological Processes, 30, 1708-1717, doi:10.1002/HYP.10730

Fassnacht, S.R., and Derry, J.E., 2009. Defining similar regions of snow in the Colorado River Basin using self-organizing maps. Water Resources Research, 46, W04507, doi:10.1029/2009WR007835.

Fassnacht, S.R., and Patterson, G.G., 2013. Niveograph Interpolation to Estimate Peak Accumulation at Two Mountain Sites. Cold and Mountain Region Hydrological Systems Under Climate Change: Towards Improved Projections (Proceedings of symposium H02, IAHS-IAPSO-IASPEI Assembly, Gothenburg, Sweden, July 2013) IAHS, 360, 59-64.

Fassnacht, S.R., May 2018. Personal communication.

Hock, R., 2003. Temperature index melt modeling in mountain areas. Journal of Hydrology, 282, 204-115, doi:10.1016/S0022-1694(03)00257-9.

Kearney, M.S., Harris, B.H., Hershbein, B., Jácome, E., and Nantz, G., 2014. In times of Drought: Nine Economic Facts about Water in the United States, Policy Memo, October 2014, The Hamilton Project, The Brookings Institution.

Löwe, H., Egli, L., Bartlett, S., Guala, M., and Manes C., 2007. On the evolution of the snow surface during snowfall. Geophysical Research Letters, 34, L21507, doi:10.1029/2007GL031637.

Ma, C. Evaluating and Correcting Sensor Change Artifacts in the SNOTEL Temperature Records, Southern Rocky Mountains, Colorado. How Sensor Change Affects Warming Trends and Modeling across Colorado. Unpublished Master's Thesis, Watershed Science Program, Colorado State University, Fort Collins, CO, USA, 2017; 43pp.

Ma, C., Fassnacht, S.R., and Kampf, S.K., 2019. How Temperature Sensor Change Affects Warming Trends and Modeling – An Evaluation across the State of Colorado. Water Resources Research, 55(11), 9748-9764. https://doi.org/10.1029/2019WR025921

Maupin, M.A., Kenny, J.F., Hutson, S.S., Lovelace, J.K., Barber, N.L., and Linsey, K.S., 2014. Estimated use of water in the United States in 2010. U.S. Geological Survey Circular 1405, 56 p., http://dx.doi.org/10.3133/cir1405.

McKinney, W., **Data Structures for Statistical Computing in Python**, Proceedings of the 9th Python in Science Conference, 51-56, 2010.

Natural Resources Conservation Service Water supply forecasting overview website. <https://www.wcc.nrcs.usda.gov/about/forecasting.html>. Accessed April 2018.

Natural Resources Conservation Service Automated snow monitoring website. <https://www.wcc.nrcs.usda.gov/about/mon_automate.html>. Accessed April 2018.

Pomery, J., Essery, R., and Toth, B., 2004. Implications of spatial distributions of snow mass and melt rate for snow-cover depletion: observations in a subarctic mountain catchment, Annals of Glaciology, 38, 195-201. https://doi.org/10.3189/172756404781814744.

Sturm, M., and Wagner, A.M., 2010. Using repeated patterns in snow distribution modeling: An arctic example, Water Resources Research, 46, https://doi.org/10.1029/2010WR009434

United States Army Corps of Engineers, 1956. Snow Hydrology; Summary report of the snow investigations. Portland OR: North Pacific Division, Corps of Engineers, U.S. Army.

Virtanen, P., Gommers, R., Oliphant, T.E., Haberland, M., Reddy, T., Cournapeau, D., Burovski, E., Peterson, P., Weckesser, W., Bright, J., Van der Walt, S. J., Brett, M., Wilson, J., Millman, J.K., Mayorov, N., Nelson, A.R.J., Jones, E., Kern, R., Larson, E., Carey, C., Polat, İ., Feng, Y., Moore, E.W., VanderPlas, J., Laxalde, D., Perktold, J., Cimrman, R., Henriksen, I., Quintero, E.A., Harris, C.R., Archibald, A.M., Ribeiro, A.H., Pedregosa, F., Van Mulbregt, P., and SciPy 1.0 Contributors, SciPy 1.0: Fundamental Algorithms for Scientific Computing in Python, 2020. *Nature Methods*, 17(3), 261-272. https://doi.org/10.1038/s41592-019-0686-2

Von Thaden B.C., Spatial accumulation patterns of snow water equivalent in the Southern Rocky Mountains. Unpublished Master's Thesis, Watershed Science Program, Colorado State University, Fort Collins, CO, USA, 2016; 41pp.

APPENDIX

A. DERIVATION OF STANDARD DEVIATION VERSUS MEAN TRAJECTORIES

A.1 DEVELOPMENT AND METHODOLOGY FOR THE REGRESSION METHOD

Three best-fit regression methods were fit to the accumulation data: linear, truncated linear (excluding mean SWE <35mm), and power for seven snow years with unique accumulation phase characteristics (Figures 1-A1 and 1-A2). The 11-day moving-average breakpoint method identified in the Methods section was used to identify the end of the accumulation phase.

The truncated linear model (Linear-1) yielded the largest coefficient of determination values in 6 of 7 years (Table A.1-1).

Table A.1-1 – Regression parameters and coefficients of determination for three regression methods based on data from seven characteristic snow years

	Linear			**Linear - 1**			**Power-2**		
	R2	**b**	**m**	**R2**	**b**	**m**	**R2**	**alpha**	**beta**
1993	0.998	3.48	0.432	0.997	6.58	0.425	0.983	0.809	0.715
1995	0.980	9.26	0.459	0.991	23.43	0.393	0.959	0.680	0.753
2002	0.986	7.26	0.431	0.989	9.13	0.419	0.986	1.260	0.608
2010	0.977	16.52	0.405	0.994	28.01	0.364	0.984	1.412	0.614
2011	0.987	11.23	0.495	0.997	29.90	0.435	0.995	1.086	0.702
2012	0.980	8.36	0.359	0.997	14.79	0.326	0.971	1.229	0.592
2013	0.987	7.56	0.450	0.995	16.64	0.406	0.991	1.257	0.623
1-(exclude SWE prior to 35 mm)									
2-(y=alpha*x^beta)									

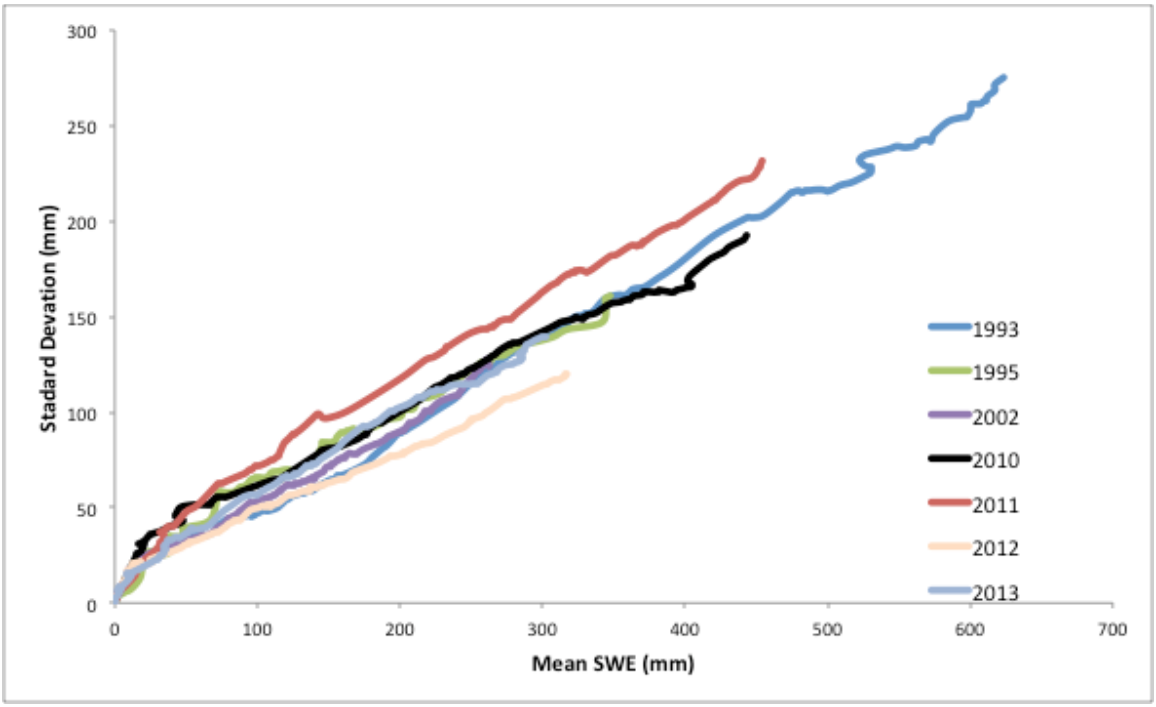

Figure A.1-1. The accumulation phase of the standard deviation versus mean SWE trajectory data set is presented for seven characteristic years. This is the data set utilized for the linear regression model.

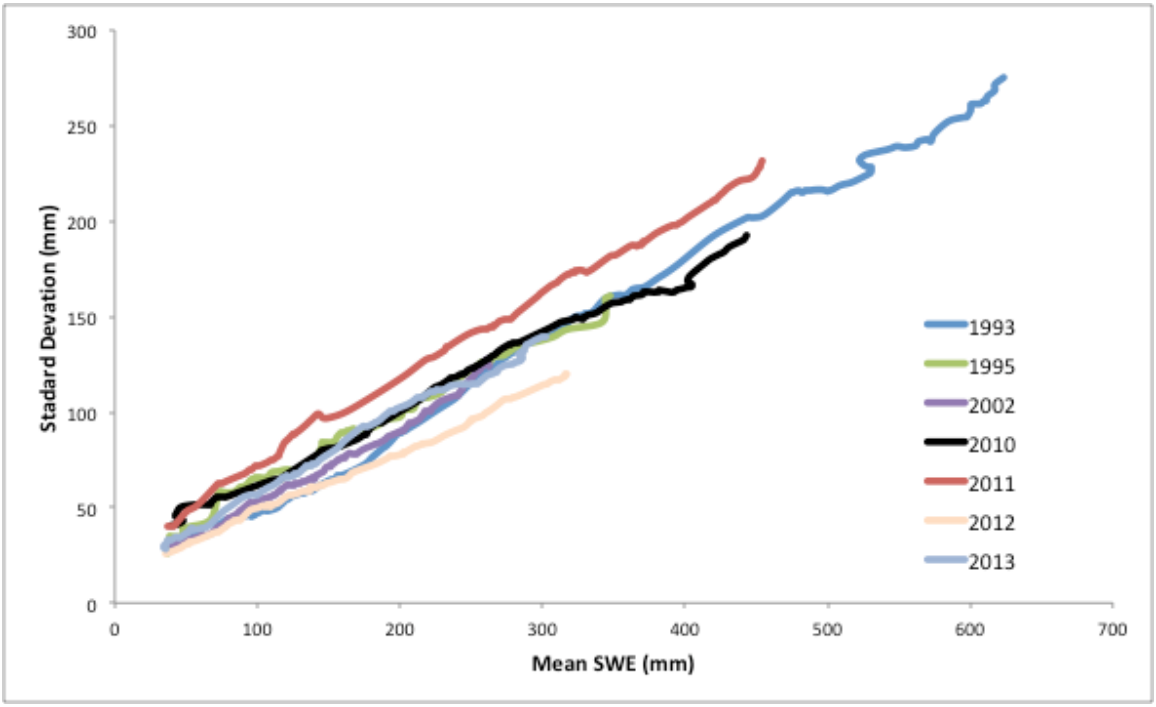

Figure A.1-2. The accumulation phase of the standard deviation versus mean SWE trajectory data set is presented for seven characteristic years. This is the data set utilized for the truncated linear regression model.

A.2 DEVELOPMENT OF INFLECTION POINT IDENTIFICATION METHOD

A variety of approaches were tested to determine a replicable method to identify the inflection point between the purely accumulation, and mixed accumulation/ablation phases, independent of the regression model applied to the accumulation phase. The three approaches tested were variations of those employed by Jonas and Egli (2009); complete linear regression for each day of the snow year, and compare regression slopes between days. Leading, lagging and centralized daily linear regression methods were tested, with date ranges varying between 10 (leading/lagging) and 11 days (central). Preliminary attempts to implement this method resulted in many false positives – changes in slope above the threshold, but much earlier than the measured accumulation phase terminated. To mitigate false positives, a minimum date threshold was included to disallow pre-emptive terminations of the accumulation phase.

After a series of preliminary analyses, two slope difference thresholds were identified for larger-scale analyses. The two slope difference thresholds (0.3 and 0.5) were tested with leading 10-day, lagging 10-day, and central 11-day methods for seven snow years. The seven years selected for testing exhibited unique characteristics on the plot of standard deviation versus mean SWE. Results were compared to the observed inflection point, which was determined through visual inspection. Based on the observed inflection point, the Nash-Sutcliffe model coefficient of efficiency was calculated to assess how accurately the predicted inflection point aligned with the observed inflection point (Table A.2-1, A.2-2, Figure A.2-1 and Figure A.2-2).

Table A.2-1 – Comparison of breakpoint prediction values of mean SWE for slope difference threshold of 0.3

	Observed mean SWE	Modeled		
Year		leading 10-day	central 11-day	lagging 10-day
1993	629	527	624	525.8
1995	411	348	347	342.1
2002	262	174	261	252.9
2010	343	414	444	390.5
2011	445	455	454	445.4
2012	317	313	316	316.4
2013	295	296	303	295.5
	NSCE	0.706	0.847	0.810
	R2	0.757	0.855	0.870

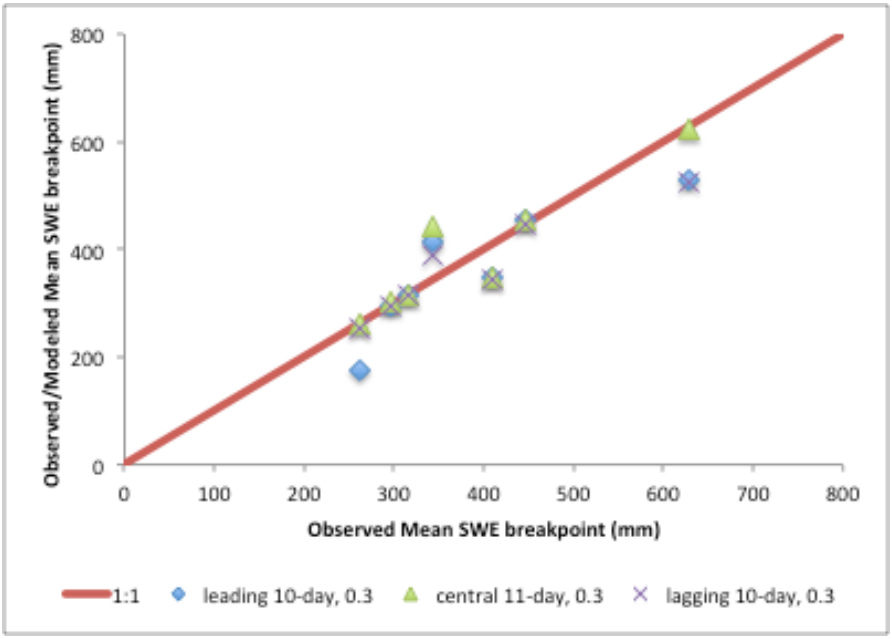

Figure A.2-1. The ideal model is represented by the one to one line, allowing the three methods (leading 10-day, central 11-day and lagging 10-day) to be compared against the ideal, visually observed inflection point mean SWE value for a slope difference threshold of 0.3.

Table A.2-2 – Comparison of breakpoint prediction values of mean SWE for slope difference threshold of 0.5

	Observed mean SWE	Modeled		
Year		leading 10-day	central 11-day	lagging 10-day
1993	629	235	628	526
1995	411	348	347	342
2002	262	259	261	256
2010	343	0	0	1
2011	445	455	454	445
2012	317	313	316	316
2013	295	294	302	297
	NSCE	0.706	0.847	0.810
	R2	0.757	0.855	0.870

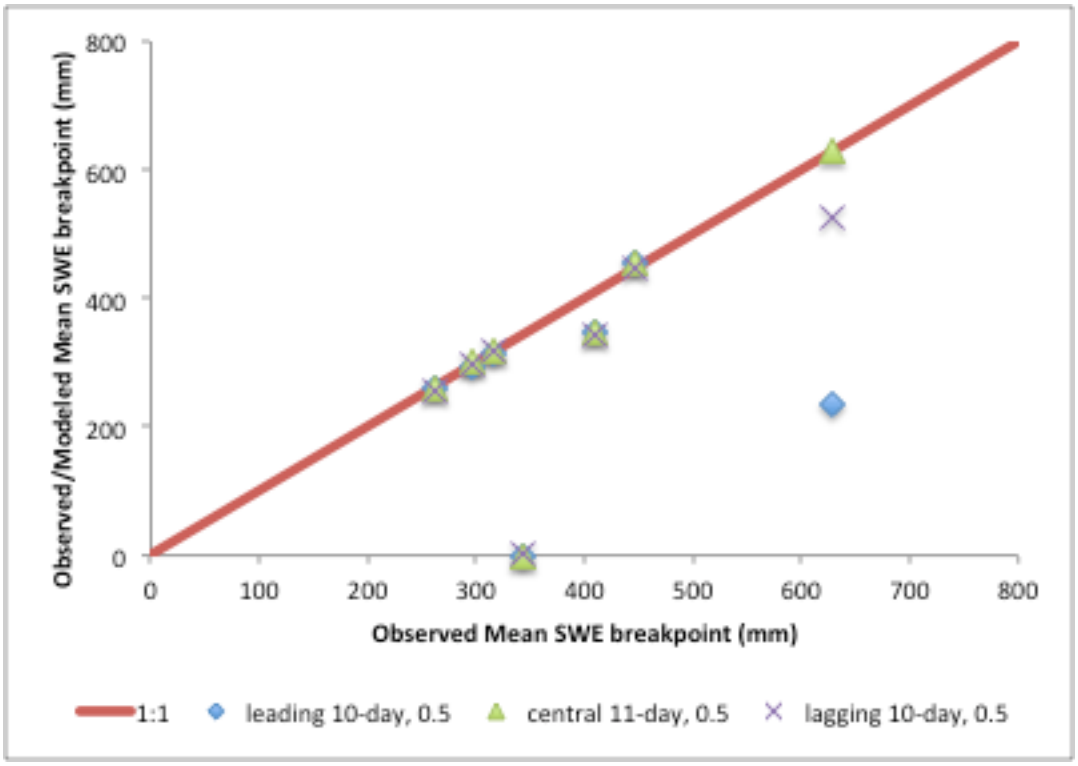

Figure A.2-2. The ideal model is represented by the one to one line, allowing the three methods (leading 10-day, central 11-day and lagging 10-day) to be compared against the ideal, visually observed inflection point mean SWE value for a slope difference threshold of 0.5.

B. DERIVATION AND EVALUATION OF ACCUMULATION SLOPES

The process of identifying inflection points, and executing a linear regression for each trajectory (34 years of data, 7 sub-sets) was simplified with development of a number of Python scripts. However, the method and parameters were not able to identify a point of inflection for 1 one instance out of 238 (0.42%). For this trajectory (north-low sub-set, 1987, Figure 2-1), the inflection point was easily identified visually, but was not detected numerically.

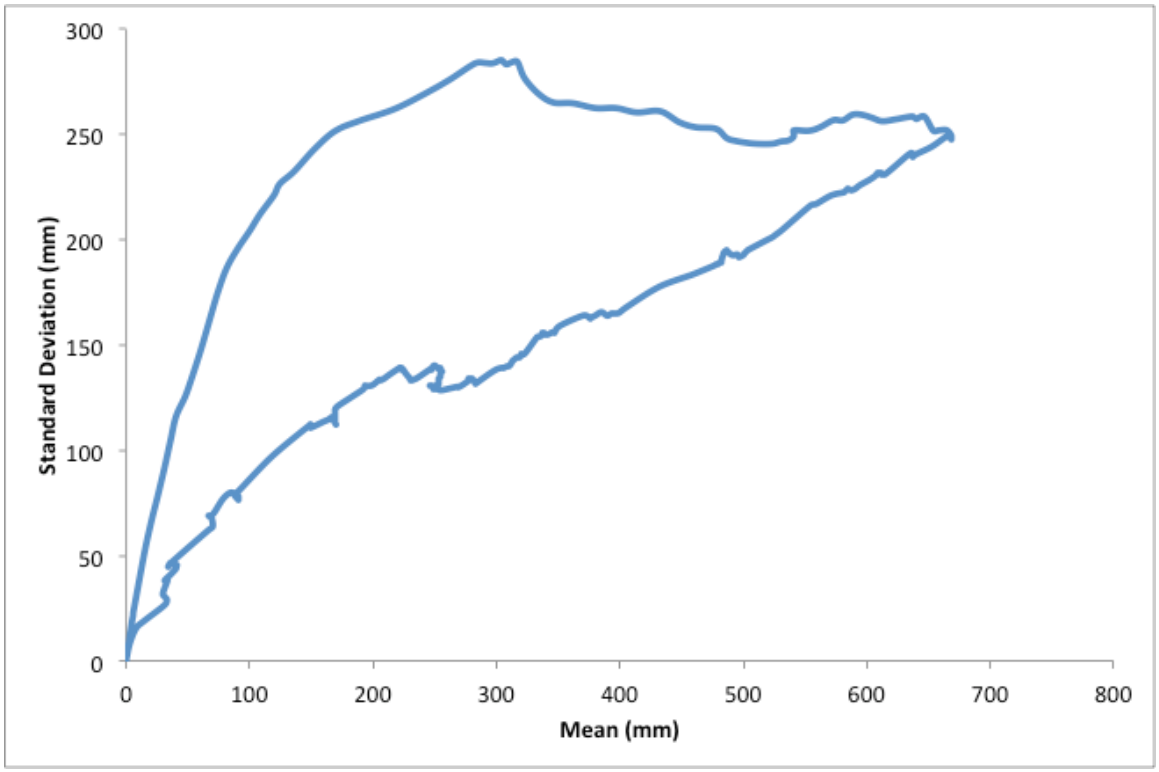

Figure B-1. The standard deviation versus mean SWE trajectory for the north-high sub-set in the snow year 1987 illustrates an un-detected sharp inflection point.

After reviewing the raw data obtained through Python scripts, nine specific instances with false inflection points were discovered. False inflection points were defined as occurring after day 250 of the water year (i.e. June, well after melt phase should have begun), and often were characterized by a coefficient of determination substantially lower than 0.7. This occurred throughout all sub-sets, over a variety of years (1 in the summary sub-set (2000), 2 in the south sub-set (2000, 2012), 2 in the north-high sub-set (1984, 2001), 2 in the south-high sub-set (1987, 2000), 2 in the south-low sub-set (2000, 2008)). The local slope near the visually observed breakpoints ranged from 0.286 to 0.465 [0.391, 0.384, 0.292, 0.322, 0.371, 0.286, 0.391, 0.465, 0.402 respectively]. The issue appeared to be more prevalent in extreme water years (5 in low, 3 in high and 1 in mid), according to the definition of water year was described in the Methods section.

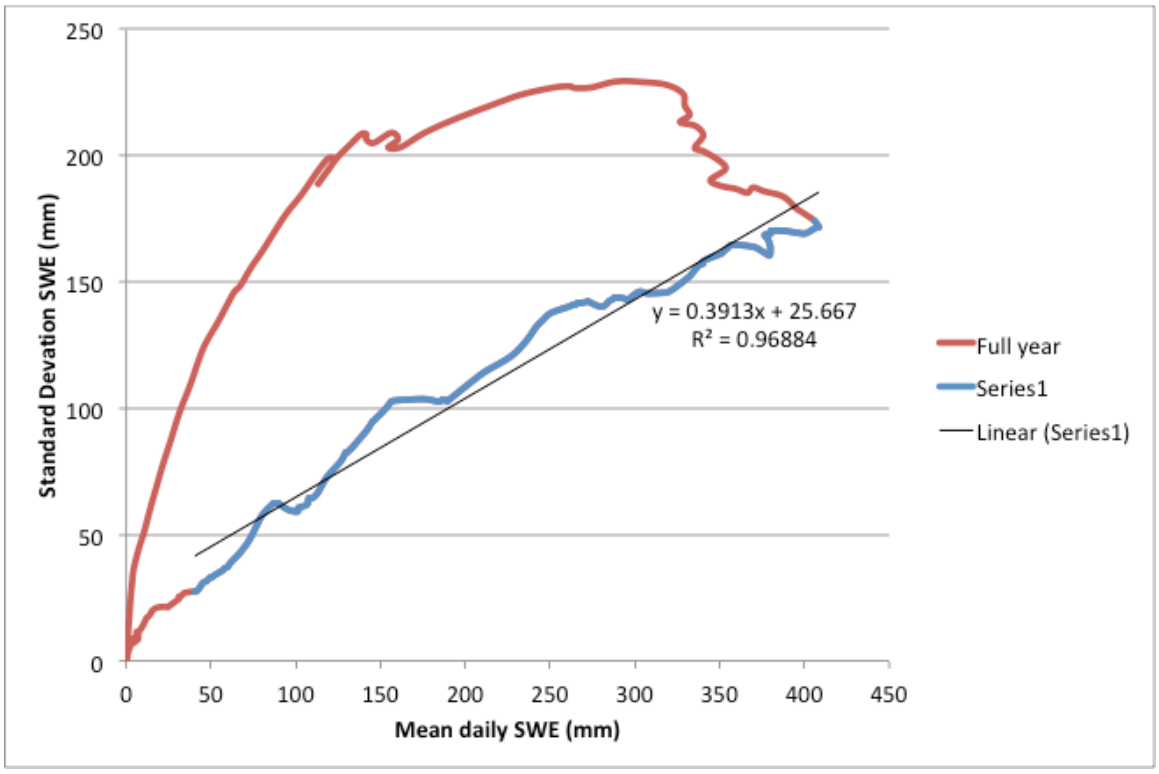

Figure B-2. The breakpoint detection methods assigned an unrealistic breakpoint and average accumulation slope for the year 2000 (summary); actual slope was 0.391.

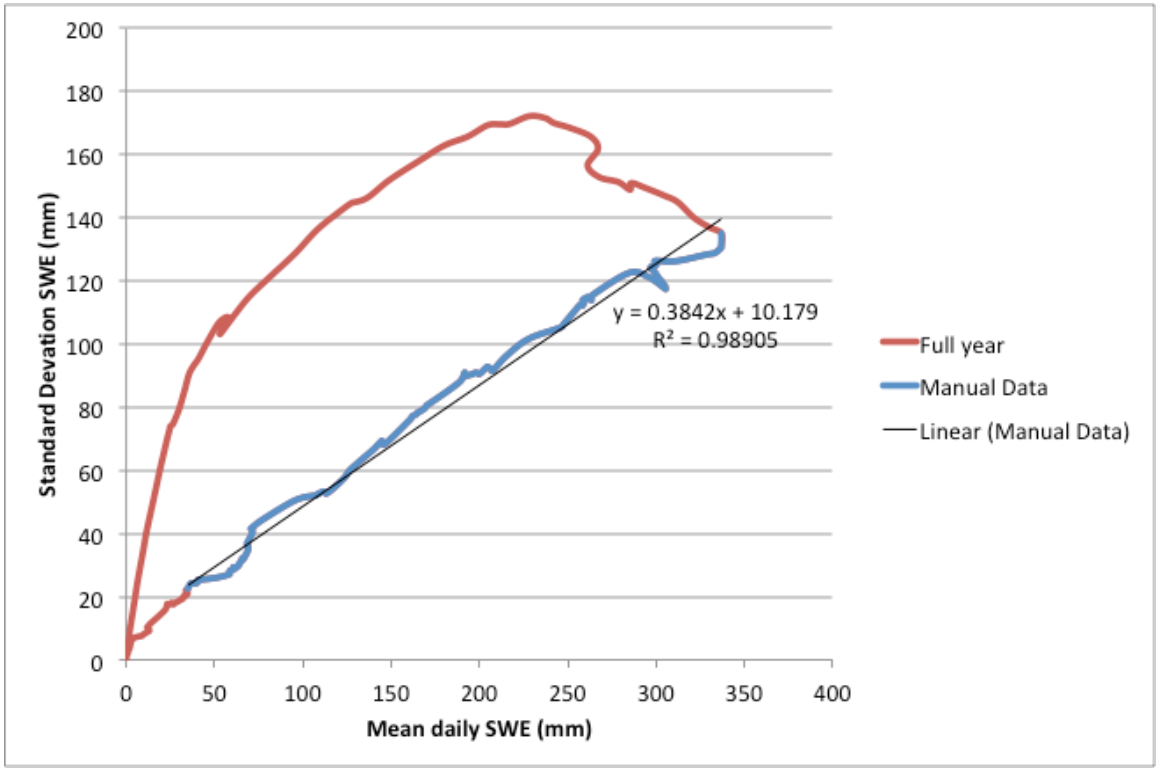

Figure B-3. The breakpoint detection methods assigned an unrealistic breakpoint and average accumulation slope for the year 2000 (south); actual slope was 0.384.

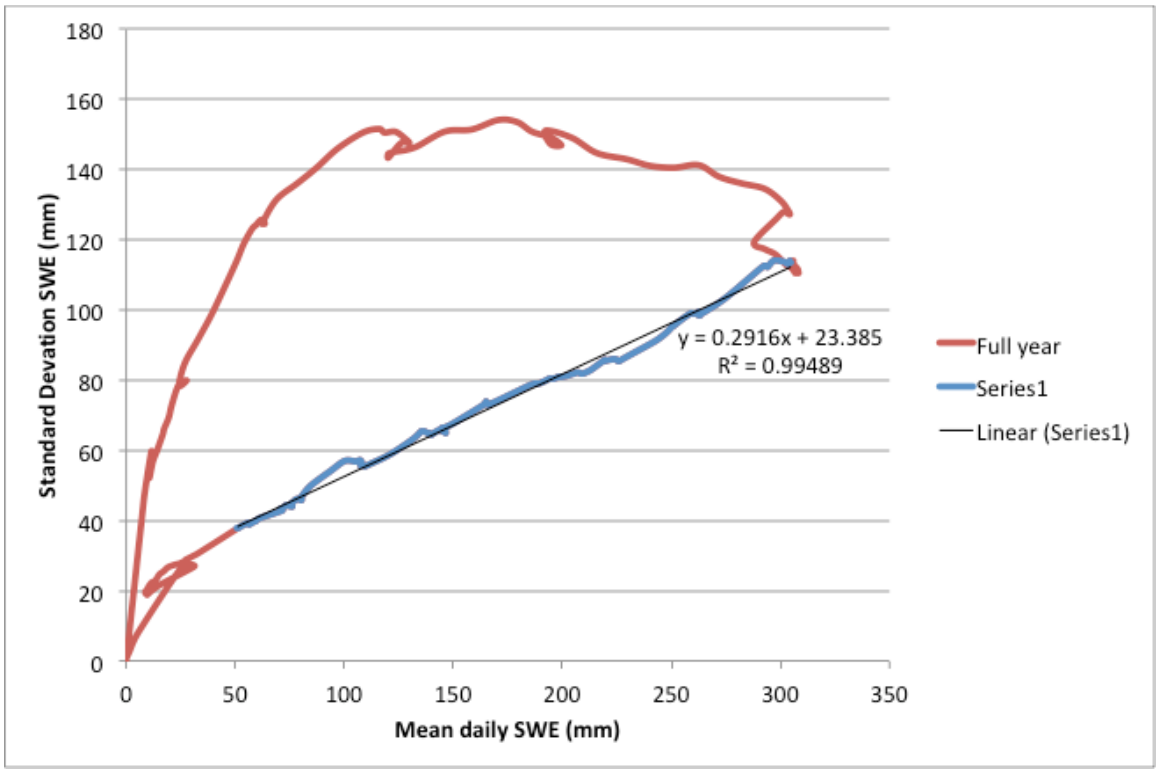

Figure B-4. The breakpoint detection methods assigned an unrealistic breakpoint and average accumulation slope for the year 2012 (south); actual slope was 0.291.

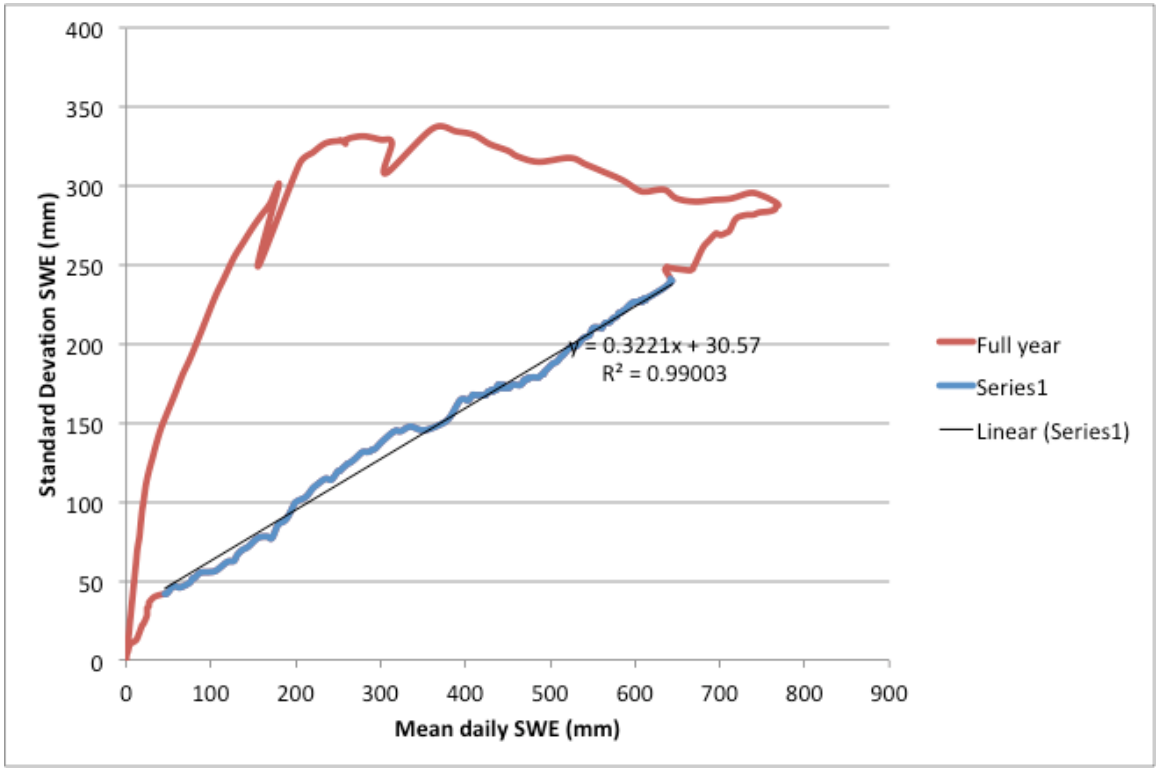

Figure B-5. The breakpoint detection methods assigned an unrealistic breakpoint and average accumulation slope for the year 1984 (north-high); actual slope was 0.322.

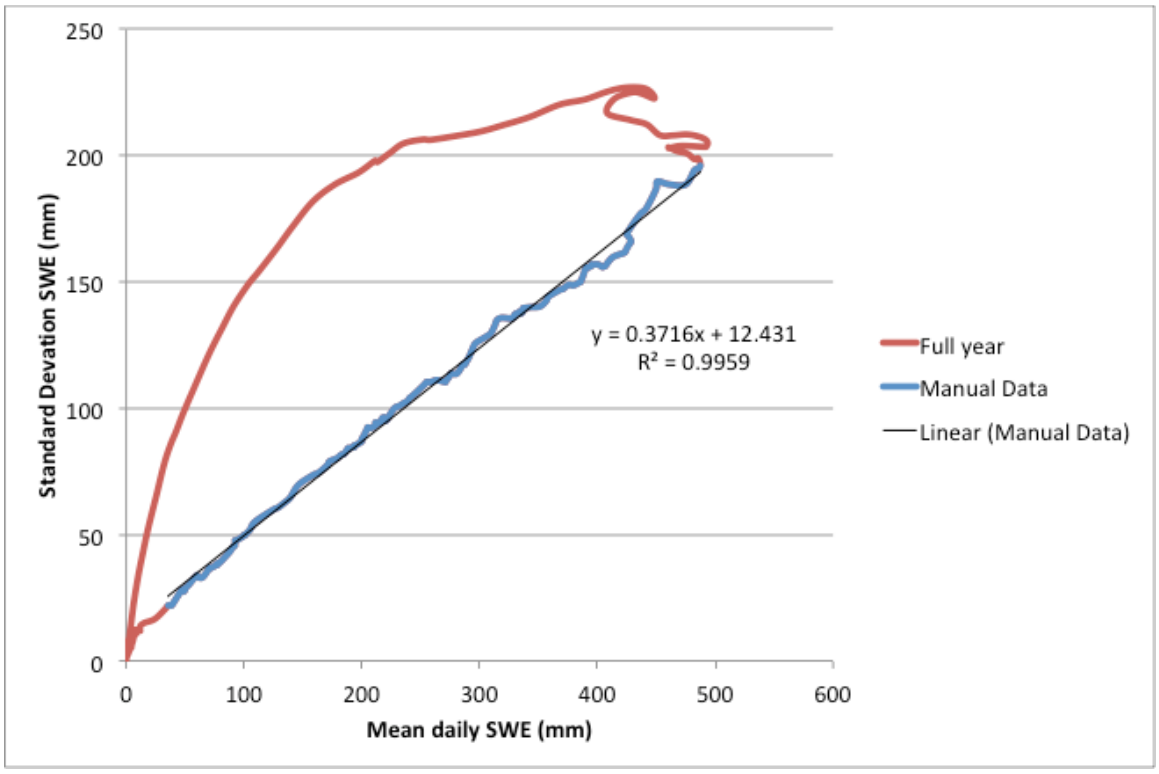

Figure B-6. The breakpoint detection methods assigned an unrealistic breakpoint and average accumulation slope for the year 2001 (north-high); actual slope was 0.371.

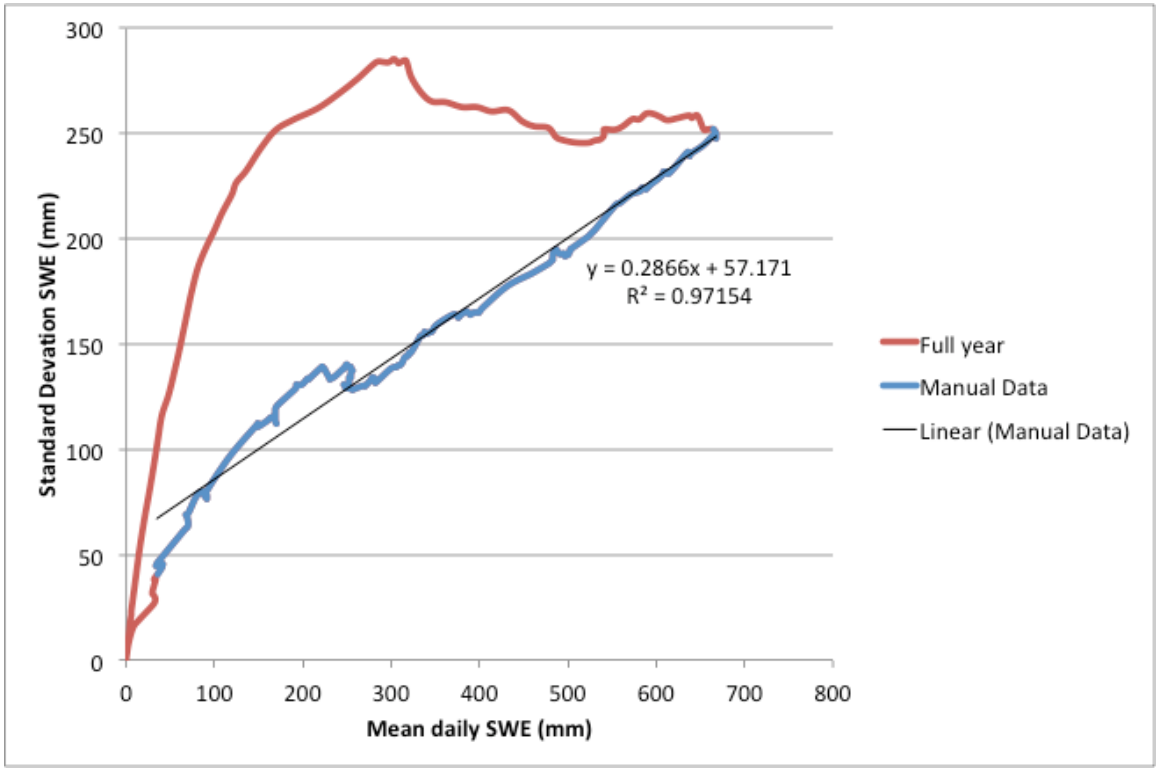

Figure B-7. The breakpoint detection methods assigned an unrealistic breakpoint and average accumulation slope for the year 1987 (south-high); actual slope was 0.286.

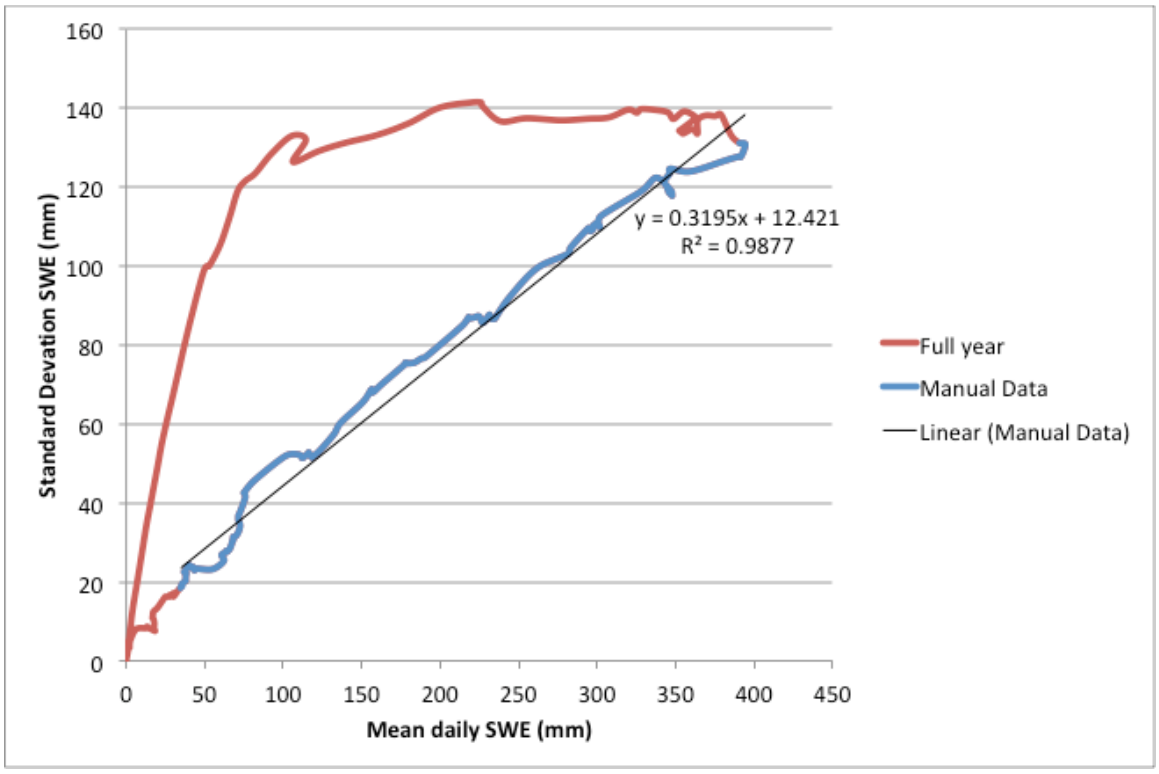

Figure B-8. The breakpoint detection methods assigned an unrealistic breakpoint and average accumulation slope for the year 2000 (south-high); actual slope was 0.319.

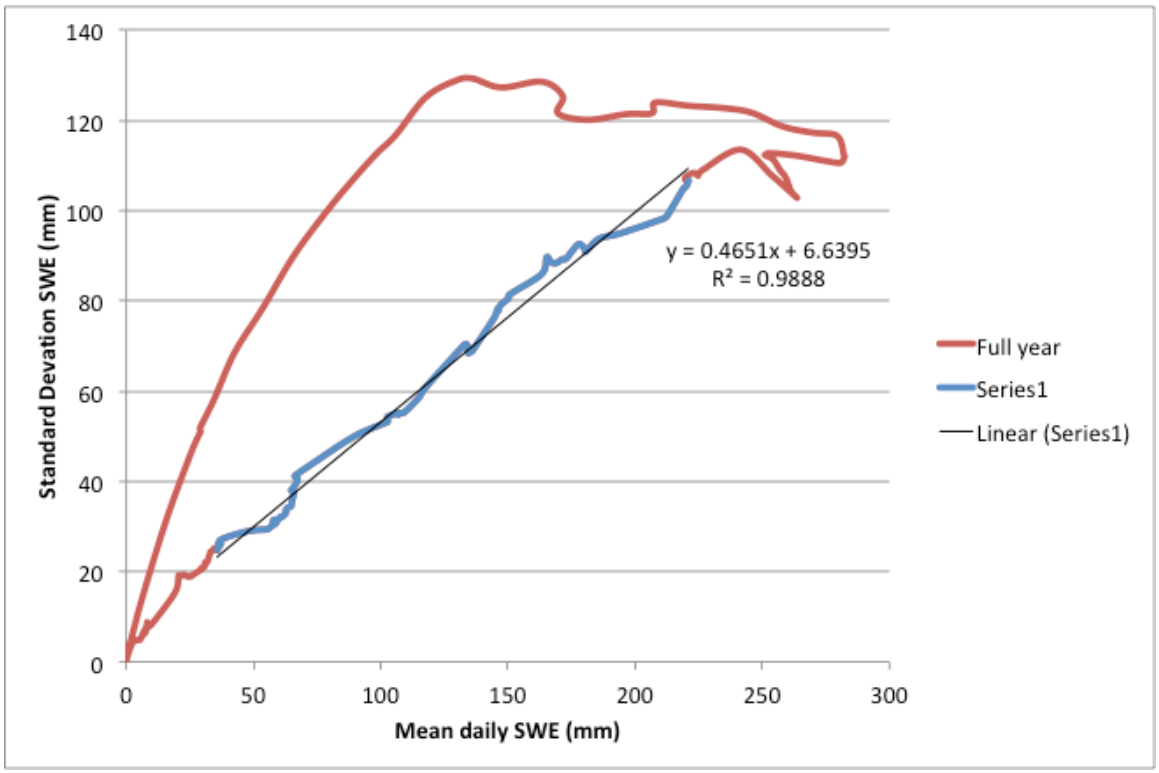

Figure B-9. The breakpoint detection methods assigned an unrealistic breakpoint and average accumulation slope for the year 2000 (south-low); actual slope was 0.465.

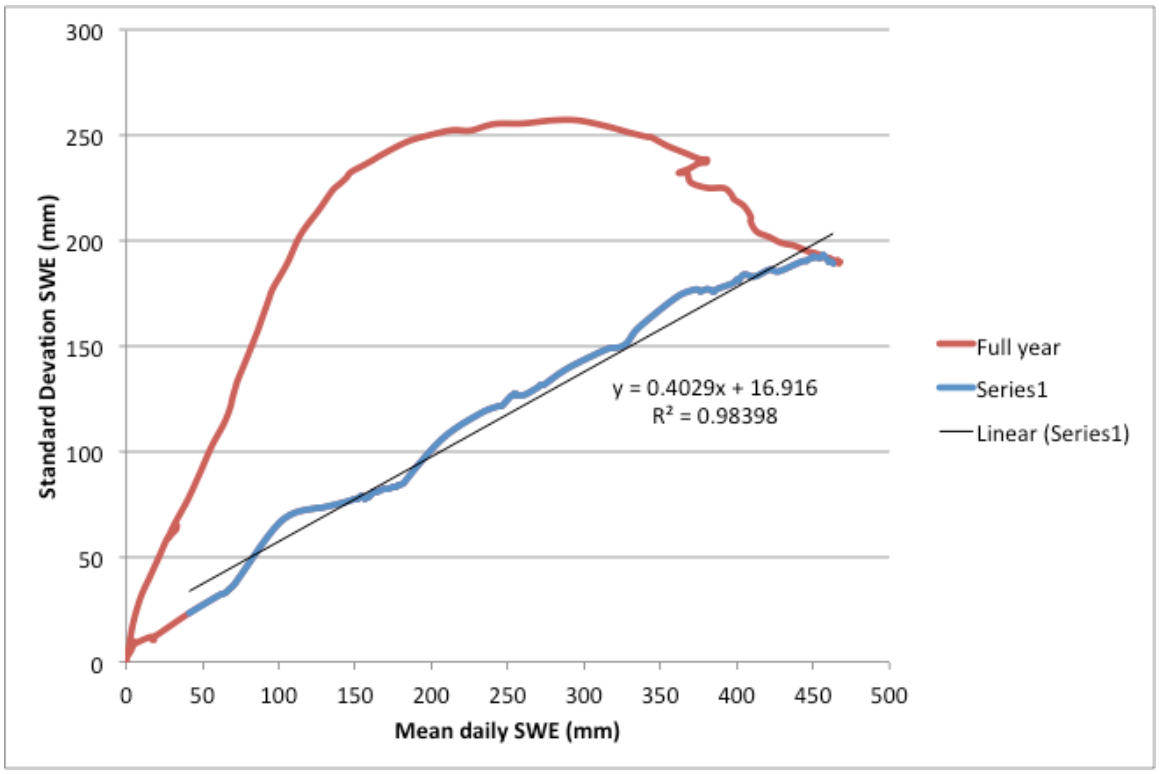

Figure B-10. The breakpoint detection methods assigned an unrealistic breakpoint and average accumulation slope for the year 2000 (south-low); actual slope was 0.402.

C. PRELIMINARY REVIEW OF ABLATION PHASE IN THE SRM

Preliminary work on the ablation phase of the standard deviation versus mean SWE trajectory was completed, and the fit of two functions were tested and compared. Both a power law and modified exponential function (Egli and Jonas (2009)) were fit to the ablation phase data from seven characteristic snow years. The Excel solver function was used to identify regression parameters for the power law function (Table C-1). Regression parameters for the modified exponential function were not calculated. Preliminary results indicate the modified exponential function more accurately represents the ablation trajectory (Figures C-1 and C-2), based on visual inspection.

Table C-1 – Curve-fitting parameters and coefficient of determination summary for ablation phase

Year	R2	alpha	beta
1993	0.972	2.76	0.539
1995	0.988	2.39	0.630
2002	0.976	2.28	0.625
2010	0.966	2.21	0.691
2011	0.978	2.43	0.657
2012	0.980	1.75	0.759
2013	0.985	2.28	0.614

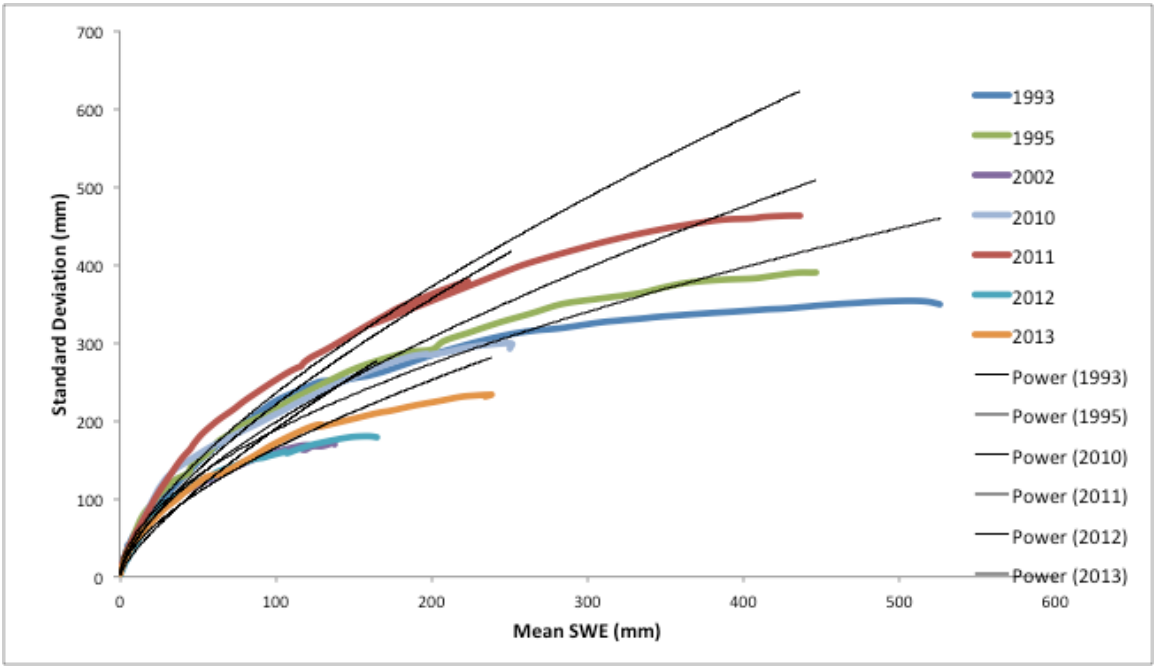

Figure C-1. The melt phase of the standard deviation versus mean SWE trajectory is presented for seven characteristic years, and illustrates the applicability of regression with the power function.

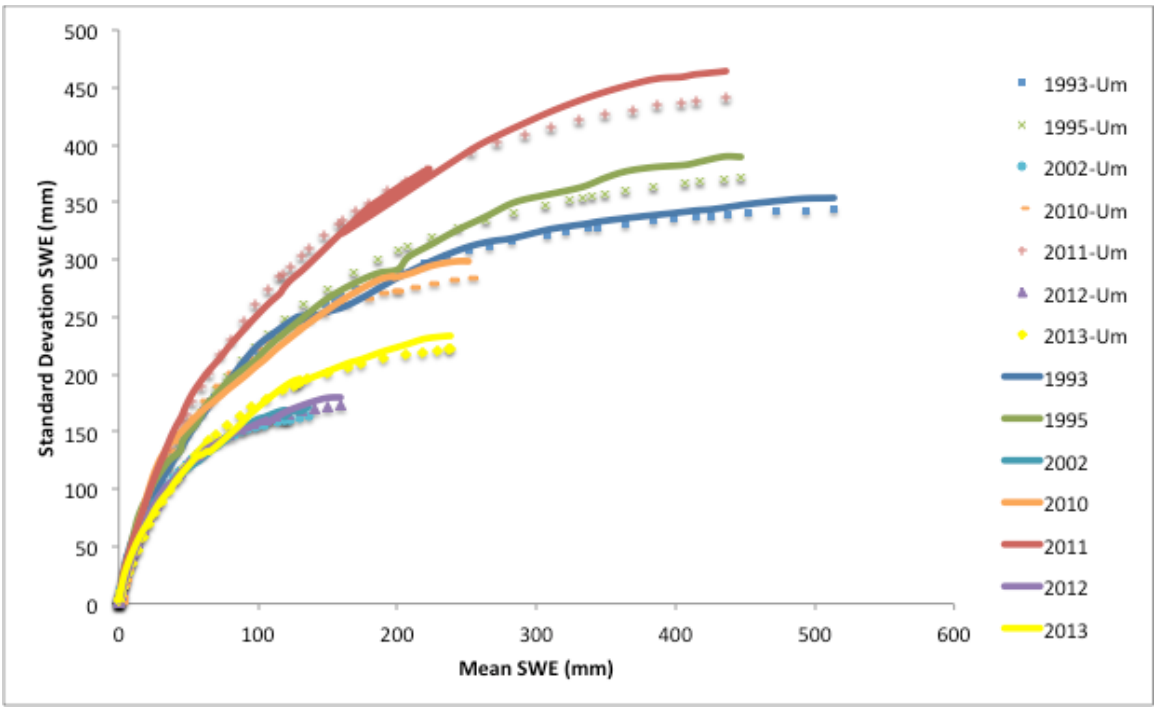

Figure C-2. The melt phase of the standard deviation versus mean SWE trajectory for the summary sub-set is included in solid lines, and the discrete points were obtained with Excel solver for the modified exponential function.

D. PRELIMINARY WORK ON IMPACT OF OCEANIC NIñO INDEX

Although conceptual in nature, preliminary visual comparisons between ONI and the annual maximum daily mean peak SWE were developed. Three-month mean Sea Surface Temperature (SST) records pertinent to the study of the ONI cycle were obtained from National Oceanic and Atmospheric Administration (NOAA) for calendar years 1950 (September-October-November, SON) through 2017 (October-November-December, OND and November-December-January (NDJ)). Calendar year data were transformed into water year data, and the SON, OND and NDJ data from the prior calendar year were included into the water year data. This was done to match up water year mean SWE records against three-month mean SST records. The relative strength rating of the ENSO cycles (very strong El Niño (EN) and strong La Niña (LN)) between water year 1982 and 2017 were analyzed (Figure D-1).

Neither strong nor consistent correlations between ONI cycles and the annual maximum daily mean peak SWE were not observed in a preliminary visual analysis of the four elevation- and latitude-based sub-sets and aggregated sub-sets. For example, ONI cycles did not appear correlated to the highest/lowest/median peak SWE values, as they are distributed sporadically between the 4^{th} and 25^{th} highest peak SWE values. When peak SWE were broken into four quadrants, variability only increased.